Dynamical Density Functional Theory with Hydrodynamic Interactions in Confined Geometries

Dynamical Density Functional Theory with Hydrodynamic Interactions in Confined Geometries

B D Goddard,[1, a)] A Nold,[2] and S Kalliadasis[2, b)]

[1)] *School of Mathematics and Maxwell Institute for Mathematical Sciences, University of Edinburgh, EH9 3FD, UK*

[2)] *Department of Chemical Engineering, Imperial College London, London, SW7 2AZ, UK*

(Dated: 11 November 2016)

We study the dynamics of colloidal fluids in both unconfined geometries and when confined by a hard wall. Under minimal assumptions, we derive a dynamical density functional theory (DDFT) which includes hydrodynamic interactions (HI; bath-mediated forces). By using an efficient numerical scheme based on pseudospectral methods for integro-differential equations, we demonstrate its excellent agreement with the full underlying Langevin equations for systems of hard disks in partial confinement. We further use the derived DDFT formalism to elucidate the crucial effects of HI in confined systems.

[a)] b.goddard@ed.ac.uk

[b)] s.kalliadasis@imperial.ac.uk

I. INTRODUCTION

We are interested in the dynamics of colloidal fluids, which consist of nano- to micrometer sized particles suspended in a viscous Newtonian fluid (known as the bath) composed of molecules much smaller and lighter than the colloidal particles. Colloidal fluids are particularly illuminating since they closely link experimental and theoretical studies of soft matter. This has been true since the work of Einstein[1], Langevin[2] and Smoluchowski[3] on the Brownian dynamics of soft matter, which was inspired by experimental observations made by Brown[4] and Perrin[5]. Such experimental observations are possible due to the characteristic length scale of soft matter systems, typically a few hundred nanometers, which enables observation by optical microscopes. In addition, modern techniques not only allow the accurate manufacture of a variety of shapes and sizes of colloidal particles, but allow the tuning of their effective interaction and their dynamics, for example by manipulation of pH or salt concentrations in the bath, or via the introduction of other species of colloidal particles.

Whilst many of the early studies of colloidal fluids were restricted to the macroscopic properties of homogeneous systems (such as diffusivities and sedimentation rates), the rapid development of microfluidics, nanotechnology, biophysics-bioengineering, chemical and process engineering and associated experimental techniques has led to much greater interest in the properties of inhomogeneous systems on a wide spectrum of lengthscales from the particle size up to the meso- and macroscopic size: from typical bath particles of size 10^{-10} m up to meters for industrial-scale vessels. At the same time colloidal systems including inhomogeneous ones are typical characterised by a wide spectrum of time scales: from 10^{-15} s between bath particle collisions up to seconds for colloidal particle diffusion. The theoretical study of such inhomogeneous systems therefore is a truly multiscale problem. The wide range of time- and lengthscales and large numbers of particles prohibit the study of such systems by particle-based methods such as Newton's equations. The first simplification typically made is to use the timescale separation between the bath dynamics (much faster) and that of the colloidal particles (much slower) to treat the bath as a continuum. This can either be done by coupling the particle dynamics to e.g. Stokes equations for the bath, or by treating the effects of the bath as noise in the colloidal particle dynamics, effectively a generalisation of Brownian motion. After this approximation, the resulting equations are computationally

tractable for a few thousand colloidal particles, but such methods still cannot tackle truly macroscopic numbers of particles. What is required is a formalism that captures important physical effects on the scale of the particle size, but is applicable to larger numbers of particles.

Here we restrict ourselves to the overdamped or high-friction regime, where, due to the action of a viscous fluid bath, the momenta of the colloidal particles may be neglected and interest lies only in their positions. In order to correctly include the effects of the flows in the bath, the motion of the particles must be coupled not only via inter-particle potentials, but also through a diffusion tensor that depends on the positions of all the colloidal particles. Many studies choose to neglect this complexity, which results in equations that are more computationally tractable, but lose crucial physics. The inclusion of this position dependence allows the modelling of hydrodynamic interactions (HI): the motion of colloidal particles through the bath causes flows in the bath, which in turn cause forces on the colloidal particles, what we have referred to as HI. For N particles in 3 dimensions, in a stochastic formulation, this requires the computation of the square root of a $3N \times 3N$ matrix (for example via Cholesky decomposition), which requires order N^3 operations. If HI are neglected, then finding this square root is trivial, but, as mentioned, neglects crucial physics. A further complication when performing numerical calculations including HI is that they are long range (e.g. decaying as the inverse of particle separation in unbounded fluids), which causes difficulties in schemes which introduce a numerical cut-off procedure.

HI are crucial in understanding the physics of many systems, for example, they have been found to be responsible for the increased viscosity of suspensions compared to a pure bath[6], the migration of polymer chains away from a wall[7], the blurring of band formation[8], and are particularly complex in confined systems[9,10] (where they depend on the wall slip condition) and for active particles and microswimmers, which produce their own HI[11].

A further complication often neglected in such studies are the effects of boundaries on the dynamics of the colloidal particles. As well as the more obvious effects of confining the colloidal particles, walls and other structures modify the flow of the bath, leading to significant changes in HI and in turn considerable changes in the dynamics of the colloidal particles. Examples of induced bath flows in unbounded and bounded geometries are shown in Figure 1. There are many applications and physical phenomena in which the inclusion of these effects is crucial, including sedimentation, adsorption and escape at boundaries,

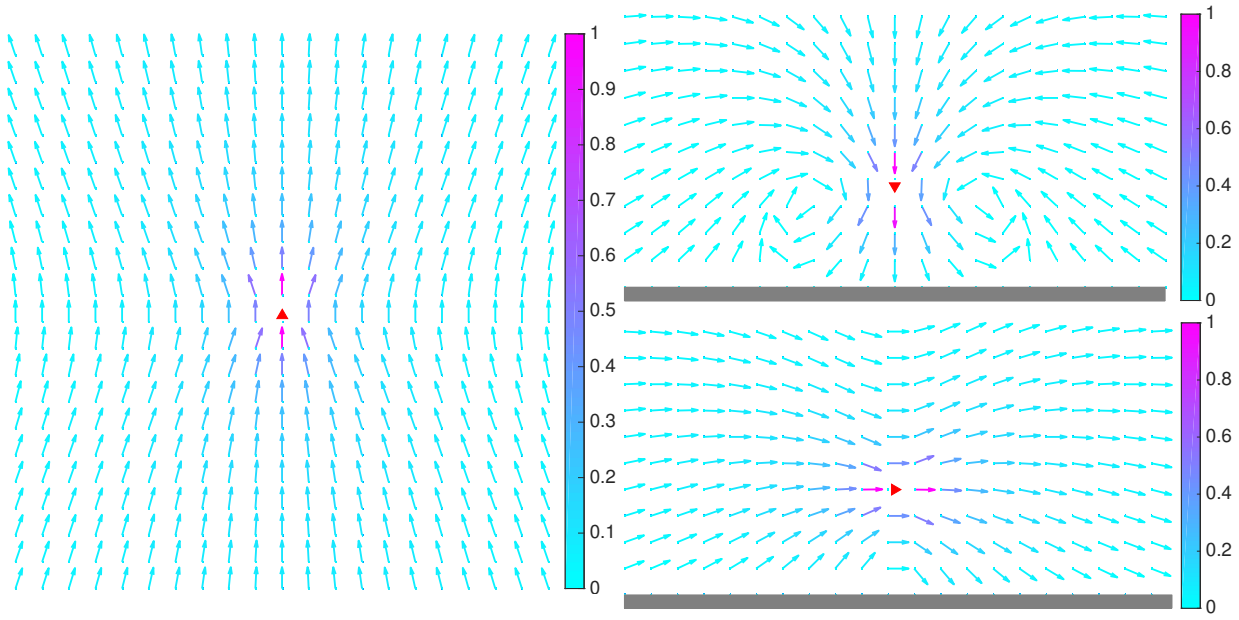

FIG. 1. Direction of forces caused by a Stokeslet (point force) acting at the position of the large red arrow. Left plot shows forces in an unbounded flow, top right for a force towards a no-slip wall and bottom right for a force parallel to a no-slip wall. Walls are marked in grey. The magnitude of the force is denoted by the colour, normalised so that the largest force shown is of norm 1. Note the rapid decay of the forces, and that at the wall they are identically zero.

resuspension by shear flow, the study of Brownian ratchets[12], flow control and particle separation in nano devices.

As discussed above, the high computational cost, especially for physically relevant numbers of particles, prevents numerical simulations of systems of interest. Hence we require a reduced model, which is not only computationally tractable, but also captures the multiscale dynamics of the problem.

One such class of reduced models are dynamical density functional theories (DDFTs). A DDFT is a statistical mechanical approach that reduces the full dynamics to closed equations for the dynamics of the one-body position density (probability of finding any particle at a given point in space at a given time). A typical DDFT is a continuity equation for the density $\rho(\mathbf{r}, t)$, with $\mathbf{r}$ a single position coordinate, i.e. $\partial_t \rho(\mathbf{r}, t) + \boldsymbol{\nabla}_{\mathbf{r}} \cdot \mathbf{J}([\rho], \mathbf{r}, t) = 0$, where the flux, $\mathbf{J}$, which is a functional of ρ, remains to be determined. The main computational benefit of a DDFT is that the dimension is fixed at the physical dimension of the system

(plus one time dimension), independently of the number of particles.

It has been shown rigorously that such DDFTs exist[13], but unfortunately the proof is non-constructive and the functional form of **J** is unknown. More recently, a new approach, termed 'power functional theory'[14] has been developed, which allows one to go beyond the adiabatic approximation made in standard DDFTs, allowing the study of systems further from equilibrium. However, in either case, practical implementations, require that a functional, or a good approximation to it, needs to be given explicitly.

Due to the widespread success of equilibrium DFT for classical fluids (see e.g. the early work of Evans[15] and Dietrich[16] and later reviews in Refs 17–19), **J** is generally based on the free energy of a related equilibrium system. This approach also ensures that the derived DDFTs agree with the static DFT at equilibrium. DDFTs for overdamped systems with no HI were first derived by Marconi and Tarazona[20] and further developed by Archer and Evans[21]. Since then, DDFTs including the inertia of the particles have been derived[22,23] and HI have been included both with[24,25] and without[26,27] inertia. There have also been extensions to multiple species[28–31], self-propelled particles[32–34], anisotropic particles[35–37], systems with confinement (excluding HI)[38,39], and external shear[40–42]. These DDFTs have been applied to a wide range of situations, including polymeric solutions[43], spinodal decomposition[21], phase separation[28], granular dynamics[22,44], nucleation[45], protein clustering[46], evaporating films[47], liquid crystals[48], microrheology in confined geometries[49], systems with temperature gradients[50], high volume fractions of hard spheres[51] and flow through constrictions[39]. Recently, a stochastic version of DDFT has been derived[52], which allows the study of energy barrier crossings, such as in nucleation.

The manuscript is laid out as follows. In Sec. II we describe HI in unconfined and confined geometries. We then outline our DDFT formalism for confined systems with HI in Sec. III. In Sec. IV we describe the numerical validation of our DDFT and demonstrate the crucial influence of HI. Finally, in Sec. VI we summarize our results and discuss some open problems and future work.

II. COLLOIDAL DYNAMICS WITH HYDRODYNAMIC INTERACTIONS

A. Smoluchowski equation for colloidal fluids

In this section we review the evolution equations for the colloidal particle positions and describe various approximations to HI in both unconfined and confined geometries. Consider a system with N spherical colloidal particles at positions $\mathbf{r}^N = (\mathbf{r}_1, \mathbf{r}_2, \ldots, \mathbf{r}_N)$ at time t. Due to the noisy effects of the bath and uncertainties in the initial positions of the particles, the dynamics are frequently described by the evolution of the N-body position probability distribution $\rho^{(N)}(\mathbf{r}^N, t)$. The governing equation for $\rho^{(N)}$ is a partial differential equation known as the Smoluchowksi equation:

$$\frac{\partial \rho^{(N)}(\mathbf{r}^N, t)}{\partial t} = \sum_{i,j=1}^{N} \boldsymbol{\nabla}_{\mathbf{r}_i} \cdot \Big(\mathbf{D}_{ij}(\mathbf{r}^N) \Big[\boldsymbol{\nabla}_{\mathbf{r}_j} + \frac{1}{k_B T} \boldsymbol{\nabla}_{\mathbf{r}_j} V(\mathbf{r}^N, t) \Big] \rho^{(N)}(\mathbf{r}^N, t) \Big). \tag{1}$$

Here V is the total potential energy and $k_B T$ is the temperature. The bath-mediated HI are described through the diffusion or mobility tensor $\mathbf{D} = (\mathbf{D}_{ij})$, which, in d spatial dimensions is a $dN \times dN$ positive definite matrix which we have decomposed into $d \times d$ blocks $\mathbf{D}_{ij}$ representing the influence of particle j on particle i.

Note that here, and from now on, we will neglect the rotational component of the motion of the particles. For a discussion of the underlying Langevin equation, the corresponding Fokker-Planck equation and the resulting DDFT, see Ref. 37. Here, since we focus on long-range HI we may safely neglect these terms; the rotational coupling decays as r_{ij}^{-3}, where r_{ij} is the interparticle separation, in comparison to the translational coupling, which decays only as r_{ij}^{-1}, see (3). Such effects are likely to become important when the particles are, on average, close together, in which case lubrication forces start to dominate (see e.g. Ref. 53). In particular, rotational effects are thought to be important when particles are sheared along a wall, and must 'roll over' each other[41].

The issue with (1) is that it is a dN-dimensional partial differential equation and so, for large numbers of particles, quickly becomes computationally intractable. Rewriting this as the equivalent system of stochastic differential equations does not mitigate the above issues of computational scaling. In Section III we will describe one way to circumvent this problem. Namely, we will derive a closed equation for the one-body position distribution, i.e. a DDFT, the computational complexity of which is independent of the number of particles. However,

before we do so it is instructive to discuss the various forms of HI commonly considered in unconfined and confined geometries.

B. Hydrodynamic interactions in unconfined geometries

HI enter the Smoluchowski equation (1) via the position-dependent diffusion tensor $\mathbf{D}$. Here we discuss the form of the diffusion tensor in an unbounded fluid and for widely-separated particles. In contrast, for particles that spend a significant proportion of their time close to other particles, the approximation of widely-separated particles breaks down and the inclusion of lubrication forces is required. We note that the inclusion of lubrication effects in DDFT is formally relatively straightforward, although standard approximations diverge as the particle separation increases (which is completely non-physical) and, as such, an arbitrary cut-off is commonly introduced. For this reason, we postpone the study of these lubrication forces in DDFT to future work, and here restrict ourselves to well-separated particles.

The following overview of the diffusion tensor is reasonably standard and in fact follows directly from the work of Oseen[53] and Rotne and Prager[54]. However, we present it here as both a starting point for the less well-known case of confined geometries, and also to highlight some of the difficulties when restricting attention to fewer than three spatial dimensions.

We consider a system of N spherical colloidal particles with no-slip boundary conditions in an unbounded, incompressible Newtonian fluid of shear viscosity η. For small, slowly-moving particles, viscous forces dominate the effects of inertia and the flow caused by the particles is described by the Stokes equation

$$\boldsymbol{\nabla}_{\mathbf{r}} p - \eta \boldsymbol{\nabla}_{\mathbf{r}}^2 \mathbf{v}(\mathbf{r}) = \mathbf{f}(\mathbf{r}) \tag{2}$$

along with the incompressibility condition

$$\boldsymbol{\nabla}_{\mathbf{r}} \cdot \mathbf{v} = 0.$$

Here p is the pressure field, $\mathbf{v}$ is the fluid velocity and $\mathbf{f}$ is the applied force at position $\mathbf{r}$.

For a point unit force at the origin (known as a Stokeslet), the Stokes equation (2) can be solved explicitly, resulting in the Oseen tensor $\mathbf{D}^{\mathrm{O}}$ with components

$$8\pi\eta D^{\mathrm{O}}_{\alpha\beta}(\mathbf{r}) = \frac{\delta_{\alpha\beta}}{r} + \frac{r_\alpha r_\beta}{r^3} \tag{3}$$

where α and β denote Cartesian coordinates (x, y or z) and $\mathbf{r} = (r_x, r_y, r_z)$ with $|\mathbf{r}| = r$. The Oseen tensor is the Green's function for the Stokes equation and describes the flow field at position $\mathbf{r}$ induced by a point particle moving due to force $\mathbf{f}$ exerted at the origin via

$$\mathbf{v} = \mathbf{D}^{\mathrm{O}}(\mathbf{r})\mathbf{f}.$$

The main approximation here is that the particle has been treated as point-like. For finite-sized spheres or disks, this approximation leads to unphysical results. For example, constructing a diffusion tensor from the Oseen tensor leads to a result that is not positive-definite for small particle separations. Since the positivity of diffusion is a result of the second law of thermodynamics, this is not only fundamentally unphysical but leads to issues when performing stochastic dynamics (see Section IV B) where one must take the square root of the diffusion tensor, which is only possible if the tensor is positive-definite[55].

To extend the result to finite-size particles one must perform an integral of the Green's function, along with a force distribution, over the particle's surface. This is generally approximated by a Taylor expansion of the Green's function known as a multipole expansion. For a spherical particle of radius a at $\mathbf{r}_j$, to first order the fluid velocity under Stokes flow for a force $\mathbf{f}_j$ applied to the particle is given by

$$\mathbf{v}(\mathbf{r}) = \Big(1 + \frac{a^2}{6}\boldsymbol{\nabla}^2_{\mathbf{r}_j}\Big)\mathbf{D}^{\mathrm{O}}(\mathbf{r} - \mathbf{r}_j)\mathbf{f}_j. \tag{4}$$

Now consider a second particle at $\mathbf{r}_i$ moving with velocity $\mathbf{v}_i$. Faxen's law[56] states that the force $\mathbf{f}_i$ exerted on particle i is proportional to the difference between its actual velocity $\mathbf{v}_i$ and the ambient fluid velocity at the position of the particle, $\mathbf{v}^{\infty}(\mathbf{r}_i)$, which is generated by the motion of the other particles. This gives

$$\mathbf{v}_i = \frac{1}{6\pi\eta a}\mathbf{f}_i + \Big(1 + \frac{a^2}{6}\boldsymbol{\nabla}^2_{\mathbf{r}_i}\Big)\mathbf{v}^{\infty}(\mathbf{r}_i). \tag{5}$$

We now note that the total fluid velocity due to the motion of all other particles is, after summing (4) over $j \neq i$, given by

$$\mathbf{v}^{\infty}(\mathbf{r}_i) = \sum_{j\neq i}\Big(1 + \frac{a^2}{6}\boldsymbol{\nabla}^2_{\mathbf{r}_j}\Big)\mathbf{D}^{\mathrm{O}}(\mathbf{r}_i - \mathbf{r}_j)\mathbf{f}_j.$$

and inserting this into (5) gives

$$\begin{aligned}\mathbf{v}_i &= \frac{1}{6\pi\eta a}\mathbf{f}_i + \sum_{j\neq i}\Big(1 + \frac{a^2}{6}\boldsymbol{\nabla}^2_{\mathbf{r}_i}\Big)\Big(1 + \frac{a^2}{6}\boldsymbol{\nabla}^2_{\mathbf{r}_j}\Big)\mathbf{D}^{\mathrm{O}}(\mathbf{r}_i - \mathbf{r}_j)\mathbf{f}_j \\ &=: \sum_j \mathbf{D}^{\mathrm{RP}}(\mathbf{r}_i, \mathbf{r}_j)\mathbf{f}_j + \mathcal{O}\big((a/r)^4\big)\end{aligned}$$

where a straightforward calculation shows that, for $\mathbf{r} = \mathbf{r}_i - \mathbf{r}_j$, and $i \neq j$,

$$\mathbf{D}^{\mathrm{RP}}(\mathbf{r}_i, \mathbf{r}_j) = \mathbf{D}^{\mathrm{RP}}(\mathbf{r}) = \mathbf{D}^{\mathrm{O}}(\mathbf{r}) + \frac{a^2}{4\pi\eta r^2}\Big(\frac{1}{3r}\mathbf{1} - \frac{\mathbf{r}\otimes\mathbf{r}}{r^3}\Big) \tag{6}$$

$$= \frac{1}{8\pi\eta}\Big[\frac{1}{r}\mathbf{1} + \frac{\mathbf{r}\otimes\mathbf{r}}{r^3} + \frac{2a^2}{r^2}\Big(\frac{1}{3r}\mathbf{1} - \frac{\mathbf{r}\otimes\mathbf{r}}{r^3}\Big)\Big], \tag{7}$$

where $\mathbf{D}^{\mathrm{O}}$ is the Oseen tensor from (3) and this result is the well-known Rotne-Prager (RP) tensor. For $i = j$ the diffusion tensor is simply given by $\mathbf{1}/(6\pi\eta a)$, which is the self-mobility of a single particle.

The main advantage of the RP description is that the resulting diffusion tensor is positive-definite for all particle separations $r > 2a$, which exactly corresponds to the case of non-overlapping hard particles of radius a. Furthermore, in three dimensions (3D), $\mathbf{D}^{\mathrm{RP}}$ is divergence free (as is the Oseen tensor (3)), which simplifies Brownian dynamics simulations (see Section IV B). However, taking the full 3D RP tensor and restricting it to two dimensions (2D) results in a tensor which is not divergence-free. The form of the 2D tensor $\mathbf{D}^{\mathrm{RP2D}}$ is identical to (7) with the vectors understood to be in 2D, but the divergence is given (see Appendix A) by

$$\boldsymbol{\nabla}_{\mathbf{r}} \cdot \mathbf{D}^{\mathrm{RP2D}}(\mathbf{r}) = -\frac{1}{8\pi\eta}\Big(\frac{1}{r^3} - \frac{2a^2}{r^5}\Big)\mathbf{r}. \tag{8}$$

We now discuss how to extend these hydrodynamic interactions to a system confined by a single hard wall.

C. Hydrodynamic interactions in confined geometries

As with the previous section, most of the results here are not new (see, for example, Refs 7, 57, and 58). However, we present them here as they do not seem to be widely known in the DDFT community, and we will require them for the derivation of the divergence of the diffusion tensor (see Section IV B and Appendix A), and thus also making our study largely self-contained. Consider a system of particles confined by a single no-slip wall at $z = 0$. Using the method of images, Blake[59] obtained the Green's function analogous to the Oseen tensor (3) as, for $i \neq j$,

$$\mathbf{D}^{\mathrm{B}}(\mathbf{r}_i, \mathbf{r}_j) = \mathbf{D}^{\mathrm{O}}(\mathbf{r}) - \mathbf{D}^{\mathrm{O}}(\mathbf{R}) + \mathbf{D}^{\mathrm{D}}(\mathbf{r}_i, \mathbf{r}_j) - \mathbf{D}^{\mathrm{SD}}(\mathbf{r}_i, \mathbf{r}_j)$$

where, as before $\mathbf{r} = \mathbf{r}_i - \mathbf{r}_j$ and, denoting the reflection in the wall of $\mathbf{r}_j = (x_j, y_j, z_j)$ by $\mathbf{r}'_j = (x_j, y_j, -z_j)$, we set $\mathbf{R} = \mathbf{r}_i - \mathbf{r}'_j$. The inclusion of the original Stokeslet, the image

Stokeslet, a Stokes doublet ($\mathbf{D}^{\mathrm{D}}$) and a source doublet ($\mathbf{D}^{\mathrm{SD}}$) ensures the no-slip boundary condition on the wall.

For the latter tensors, it is convenient to express them as their coordinate entries:

$$8\pi\eta\mathbf{D}^{\mathrm{D}}_{\alpha\beta}(\mathbf{r}_i,\mathbf{r}_j) = 2z_j^2(1-2\delta_{\beta z})\Big(\frac{\delta_{\alpha\beta}}{R^3} - 3\frac{R_\alpha R_\beta}{R^5}\Big)$$
$$8\pi\eta\mathbf{D}^{\mathrm{SD}}_{\alpha\beta}(\mathbf{r}_i,\mathbf{r}_j) = 2z_j(1-2\delta_{\beta z})\Big(\frac{\delta_{\alpha\beta}R_z}{R^3} - \frac{\delta_{\alpha z}R_\beta}{R^3} + \frac{\delta_{\beta z}R_\alpha}{R^3} - 3\frac{R_\alpha R_\beta R_z}{R^5}\Big).$$

As before, to second order in $a/\min(r,R)$, we find

$$\mathbf{D}^{\mathrm{RPB}}(\mathbf{r}_i,\mathbf{r}_j) = \Big(1+\frac{a^2}{6}(\boldsymbol{\nabla}^2_{\mathbf{r}_i}+\boldsymbol{\nabla}^2_{\mathbf{r}_j})\Big)\mathbf{D}^{\mathrm{B}}(\mathbf{r}_i,\mathbf{r}_j)$$

from which, using the same argument as in the unbounded case, it easily follows that

$$\mathbf{D}^{\mathrm{RPB}}(\mathbf{r}_i,\mathbf{r}_j) = \mathbf{D}^{\mathrm{RP}}(\mathbf{r}) - \mathbf{D}^{\mathrm{RP}}(\mathbf{R}) + \Delta\mathbf{D}(\mathbf{r}_i,\mathbf{r}_j) \tag{9}$$

where

$$\Delta\mathbf{D}(\mathbf{r}_i,\mathbf{r}_j) = \Big(1+\frac{a^2}{6}(\boldsymbol{\nabla}^2_{\mathbf{r}_i}+\boldsymbol{\nabla}^2_{\mathbf{r}_j})\Big)\big(\mathbf{D}^{\mathrm{D}}(\mathbf{r}_i,\mathbf{r}_j) - \mathbf{D}^{\mathrm{SD}}(\mathbf{r}_i,\mathbf{r}_j)\big)$$

Denoting $\mathbf{R} = (R_x, R_y, R_z)$ and taking $\alpha \neq \beta \in \{x, y\}$ we find the entries of $\Delta\mathbf{D}$ to be

$$\Delta\mathbf{D}_{\alpha\alpha}(\mathbf{r}_i,\mathbf{r}_j) = \frac{1}{4\pi\eta}\Big[\frac{-z_iz_j}{R^3}\Big(1-3\frac{R_\alpha^2}{R^2}\Big) + \frac{a^2R_z^2}{R^5}\Big(1-5\frac{R_\alpha^2}{R^2}\Big)\Big]$$
$$\Delta\mathbf{D}_{zz}(\mathbf{r}_i,\mathbf{r}_j) = \frac{1}{4\pi\eta}\Big[\frac{z_iz_j}{R^3}\Big(1-3\frac{R_z^2}{R^2}\Big) - \frac{a^2R_z^2}{R^5}\Big(3-5\frac{R_z^2}{R^2}\Big)\Big]$$
$$\Delta\mathbf{D}_{\alpha\beta}(\mathbf{r}_i,\mathbf{r}_j) = \frac{1}{4\pi\eta}\Big[\frac{3z_iz_jR_\alpha R_\beta}{R^5} - \frac{5a^2R_\alpha R_\beta R_z^2}{R^7}\Big]$$
$$\Delta\mathbf{D}_{\alpha z}(\mathbf{r}_i,\mathbf{r}_j) = \frac{1}{4\pi\eta}\Big[\frac{z_jR_\alpha}{R^3}\Big(1-3\frac{z_iR_z}{R^2}\Big) - \frac{a^2R_\alpha R_z}{R^5}\Big(2-5\frac{R_z^2}{R^2}\Big)\Big]$$
$$\Delta\mathbf{D}_{z\alpha}(\mathbf{r}_i,\mathbf{r}_j) = \frac{1}{4\pi\eta}\Big[\frac{z_jR_\alpha}{R^3}\Big(1+3\frac{z_iR_z}{R^2}\Big) - \frac{5a^2R_\alpha R_z^3}{R^7}\Big].$$

Note that the above expression holds for $i \neq j$ and it remains to determine the corresponding expression for $i = j$, i.e. the self-mobility of a single particle in the presence of a no-slip wall. Since the diffusion tensor above has been derived by considering the image of the source, in order to ensure the validity of the no-slip condition of the wall, we do the same for a single particle, the mobility of which is affected by the distance to its own image (equivalently the distance to the wall). The distance to the image is given by the length of the vector $\mathbf{R} = \mathbf{r}_i - \mathbf{r}'_i = (0, 0, 2z)$. We note that the Oseen tensor is singular at $r = 0$, but this is not an issue as the correct term to take for the $i = j$ case is $\mathbf{1}/(6\pi\eta a)$, as described above.

A straightforward calculation then shows that we may split the mobility into terms parallel and perpendicular to the wall (i.e. the off-diagonal elements of $\mathbf{D}^{\mathrm{RPB}}$ vanish) and we find

$$\mathbf{D}^{\mathrm{RPB}}_{\mathrm{self}} = \begin{pmatrix} D_{\parallel} & 0 & 0 \\ 0 & D_{\parallel} & 0 \\ 0 & 0 & D_{\perp} \end{pmatrix} \tag{10}$$

where

$$D_{\parallel} = \frac{1}{6\pi\eta}\Big(1 - \frac{9a}{16z} + \frac{1}{8}\Big(\frac{a}{z}\Big)^3\Big) + \mathcal{O}\big((a/z)^3\big)$$
$$D_{\perp} = \frac{1}{6\pi\eta}\Big(1 - \frac{9a}{8z} + \frac{1}{2}\Big(\frac{a}{z}\Big)^3\Big) + \mathcal{O}\big((a/z)^3\big).$$

We note that going to the RP level is once again crucial in order to obtain the correct physics. In particular, truncating $D_{\perp}$ to first order results in a diffusion coefficient that changes sign from positive to negative as the wall is approached, which is clearly unphysical. One further consideration is the neglect of lubrication forces, which modify the self-mobilities close to the wall. Whilst there are exact expressions for these[9,60,61] as in Ref. 58, we choose to be consistent in approximating all terms at the RP level, and note that the differences are only significant for $z < 2a$. In the small-z limit, one expects the continuum approximation to break down, since individual particles have a non-vanishing mobility even when in contact with the surface. However, we do not expect this approximation to have a significant effect on the results.

Finally, we combine the above results for a confining wall into a single diffusion tensor

$$\mathbf{D}_{ij}(\mathbf{r}_i, \mathbf{r}_j) = \delta_{ij}\mathbf{D}^{\mathrm{RPB}}_{\mathrm{self}}(z_i) + (1 - \delta_{ij})\mathbf{D}^{\mathrm{RPB}}(\mathbf{r}_i, \mathbf{r}_j),$$

which we will refer to as the Rotne-Prager-Blake (RPB) formalism. As a natural extension to the work of Rex and Löwen[26], in the following we will treat a slightly more general form for the diffusion tensor, namely

$$\mathbf{D}_{ij}(\mathbf{r}^N) = \delta_{ij}\mathbf{D}^{(0)}(\mathbf{r}_i) + \delta_{ij}\sum_{k\neq i}\mathbf{D}^{(1)}(\mathbf{r}_i, \mathbf{r}_k) + (1 - \delta_{ij})\mathbf{D}^{(2)}(\mathbf{r}_i, \mathbf{r}_j). \tag{11}$$

Here $\mathbf{D}^{(1)}$ and $\mathbf{D}^{(2)}$ are arbitrary 3×3 tensors.

D. Partial confinement

As well as confinement by walls, we are also interested in the effects of confining the motion of the colloidal particles to 1D or 2D in a 3D bath. This situation is both physically

interesting (see below) and numerically more tractable than solving the full 3D equations for the colloidal particles. There are two main ways in which such a confined situation can arise.

1. Both the bath and colloids are confined to 2D: It is known that the transport coefficients in 2D fluids are not well-defined[62], which is a result of the slow decay of the hydrodynamic modes. In addition, the Stokes approximation to the Navier-Stokes equations does not hold in unbounded 2D fluids and HI show a strong dependence on the size of the system[63].

2. Colloids are confined to 2D but the bath flows in 3D. This is known as partial confinement, and is the situation we will study here. It applies when the colloidal particles are trapped at a planar interface, but the fluid bath remains free to flow in 3D. Such a trapping can be realised either due to the colloids being at the interface between two fluid domains, or due to external forces such as those applied by optical tweezers. We will assume in the following that the trapping mechanism does not affect the flow in the bath. A schematic of the 2D partial confinement of the colloidal particles and associated 3D flows in the bath is shown in Figure 2.

We note that, although the restriction to 2D simplifies the numerics, especially for DDFT, it introduces an extra complexity for the stochastic dynamics, namely that the flow is not incompressible when restricted to 2D, and so the resulting diffusion tensor is not divergence-free (see Appendix A). It should also be emphasised that it is possible to perform experiments in 2D, e.g. using superparamagnetic colloids[64,65]

III. DYNAMICAL DENSITY FUNCTIONAL THEORY

We now outline the derivation of a DDFT, which reduces equation (1) with diffusion tensor (11) to a closed equation for the one-body density

$$\rho(\mathbf{r},t) = N\int \mathrm{d}\mathbf{r}^{N-1}\rho^{(N)}(\mathbf{r}^N,t),$$

where we use $\mathrm{d}\mathbf{r}^{N-k}$ to denote $\mathrm{d}\mathbf{r}_{k+1}\ldots\mathrm{d}\mathbf{r}_N$. It is convenient to define the k-body densities

$$\rho^{(k)}(\mathbf{r},t) = \frac{N!}{(N-k)!}\int \mathrm{d}\mathbf{r}^{N-k}\rho^{(N)}(\mathbf{r}^N,t),$$

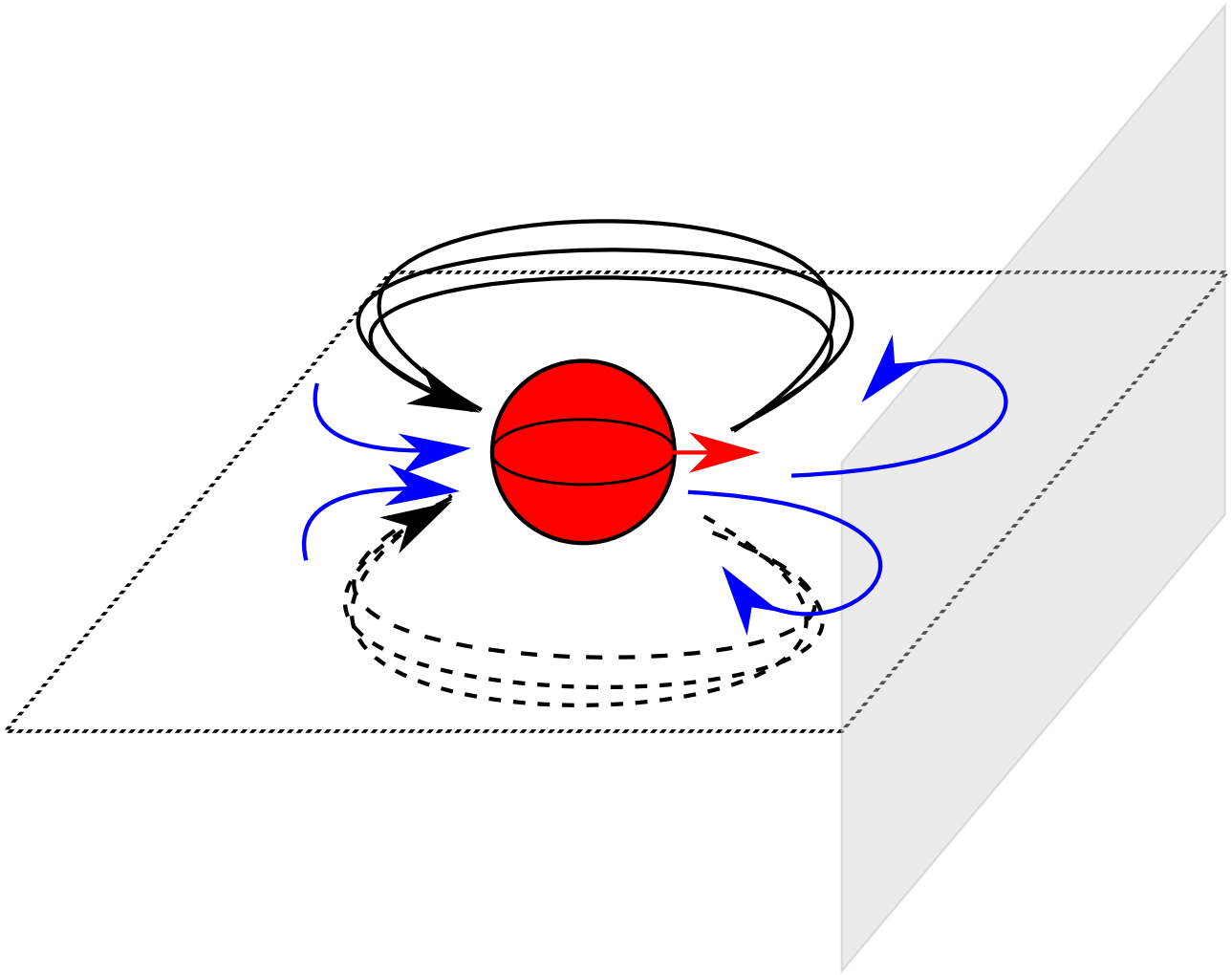

FIG. 2. Schematic of hydrodynamic interactions in a partially confined system. Colloid particles (red) are confined to a plane; their motion (red arrow) induces 3D flows in the bath, which separate into planar effects (blue) and out-of-plane effects (black). The flows are further affected by a wall (grey).

where for ease of notation we drop the superscript when $k = 1$.

The general strategy is to multiply the Smoluchowski equation (1) by N and integrate over all positions except $\mathbf{r}_1$. We then use the symmetry of $\rho^{(N)}$ and V under interchange of particles to simplify the expressions. It remains to write the term involving the N-body potential as a functional of ρ. For this we follow Rex and Löwen[26] and introduce a fictitious additional external potential $U(\mathbf{r}, t)$, such that at time $t = t_0$, under the modified external potential $V(\mathbf{r}^N, t) + \sum_{n=1}^{N} U(\mathbf{r}_n, t_0)$, the system with instantaneous density $\rho(\mathbf{r}, t_0)$ is at

equilibrium. This allows us to write the gradient of U in terms of the excess free energy of the equilibrium system, which is a functional of ρ. We then finally rewrite the two-body densities $\rho^{(2)}$ in terms of ρ, assuming that the equilibrium expression for the nonequilibrium two-body density may be employed via the adiabatic approximation.

This derivation is a generalisation of the results of Rex and Löwen[26], both in that it includes a position-dependent self-mobility as well as N-body potentials. Further details of the calculation are given in Appendix B and here we simply state the result:

$$\begin{aligned}\frac{\partial\rho(\mathbf{r}_1,t)}{\partial t} = \frac{1}{k_BT}\boldsymbol{\nabla}_{\mathbf{r}_1}\cdot\Big(&\mathbf{D}^{(0)}(\mathbf{r}_1)\rho(\mathbf{r}_1,t)\boldsymbol{\nabla}_{\mathbf{r}_1}\frac{\delta\mathcal{F}[\rho]}{\delta\rho(\mathbf{r}_1,t)}\\ &+\int \mathrm{d}\mathbf{r}_2\mathbf{D}^{(1)}(\mathbf{r}_1,\mathbf{r}_2)\rho^{(2)}(\mathbf{r}_1,\mathbf{r}_2)\boldsymbol{\nabla}_{\mathbf{r}_1}\frac{\delta\mathcal{F}[\rho]}{\delta\rho(\mathbf{r}_1,t)}\\ &+\int \mathrm{d}\mathbf{r}_2\mathbf{D}^{(2)}(\mathbf{r}_1,\mathbf{r}_2)\rho^{(2)}(\mathbf{r}_1,\mathbf{r}_2)\boldsymbol{\nabla}_{\mathbf{r}_2}\frac{\delta\mathcal{F}[\rho]}{\delta\rho(\mathbf{r}_2,t)}\Big).\end{aligned} \tag{12}$$

This reduces to the case studied by Rex and Löwen under the restrictions that $\mathbf{D}^{(0)}$ is a multiple of the identity matrix, that $\mathbf{D}^{(1)}(\mathbf{r}_1,\mathbf{r}_2)$ and $\mathbf{D}^{(2)}(\mathbf{r}_1,\mathbf{r}_2)$ are actually functions of $\mathbf{r}_1-\mathbf{r}_2$, and that the inter-particle potential is two-body.

In order to obtain a DDFT we need to determine, or approximate, the functional dependence of $\rho^{(2)}$ on ρ. This may be done by solving the exact generalised Ornstein-Zernike equation

$$\begin{aligned}\rho^{(2)}(\mathbf{r}_1,\mathbf{r}_2,t) = &\big(1+c^{(2)}(\mathbf{r}_1,\mathbf{r}_2)\big)\rho(\mathbf{r}_1,t)\rho(\mathbf{r}_2,t)\\ &+\rho(\mathbf{r}_2,t)\int \mathrm{d}\mathbf{r}_3\big(\rho^{(2)}(\mathbf{r}_1,\mathbf{r}_3,t)-\rho(\mathbf{r}_1,t)\rho(\mathbf{r}_3,t)\big)c^{(2)}(\mathbf{r}_3,\mathbf{r}_2),\end{aligned} \tag{13}$$

where

$$c^{(2)}(\mathbf{r}_1,\mathbf{r}_2) = \frac{\delta^2\mathcal{F}_{\mathrm{ex}}[\rho]}{\delta\rho(\mathbf{r}_1,t)\delta\rho(\mathbf{r}_2,t)}.$$

Whilst this is an exact relationship, it is computationally very demanding as the Ornstein-Zernike equation must be solved at every time step. A simpler approach, which has been shown to be accurate in a range of systems[24,25,31] is to make the approximation

$$\rho^{(2)}(\mathbf{r}_1,\mathbf{r}_2) = \rho(\mathbf{r}_1,t)\rho(\mathbf{r}_2,t)g(\mathbf{r}_1,\mathbf{r}_2,[\rho]), \tag{14}$$

where it is assumed that (a good approximation to) the correlation function g is known explicitly. It is this route that we choose in the present work, leading to a DDFT of the

form

$$\frac{\partial\rho(\mathbf{r}_1,t)}{\partial t} = \frac{1}{k_BT}\boldsymbol{\nabla}_{\mathbf{r}_1}\cdot\Big(\mathbf{D}^{(0)}(\mathbf{r}_1)\rho(\mathbf{r}_1)\boldsymbol{\nabla}_{\mathbf{r}_1}\frac{\delta\mathcal{F}[\rho]}{\delta\rho(\mathbf{r}_1,t)} + \int \mathrm{d}\mathbf{r}_2\mathbf{D}^{(1)}(\mathbf{r}_1,\mathbf{r}_2)\rho(\mathbf{r}_1,t)\rho(\mathbf{r}_2,t)g(\mathbf{r}_1,\mathbf{r}_2,[\rho])\boldsymbol{\nabla}_{\mathbf{r}_1}\frac{\delta\mathcal{F}[\rho]}{\delta\rho(\mathbf{r}_1,t)} + \int \mathrm{d}\mathbf{r}_2\mathbf{D}^{(2)}(\mathbf{r}_1,\mathbf{r}_2)\rho(\mathbf{r}_1,t)\rho(\mathbf{r}_2,t)g(\mathbf{r}_1,\mathbf{r}_2,[\rho])\boldsymbol{\nabla}_{\mathbf{r}_2}\frac{\delta\mathcal{F}[\rho]}{\delta\rho(\mathbf{r}_2,t)}\Big). \tag{15}$$

It is worth noting that in order to be consistent with the adiabatic approximation, one should solve (13) at each step of the dynamics. However, due to the large computational demands of this, we instead choose to use a simple choice of g in (14). Namely, for hard spheres or disks of radius a, we choose $g(\mathbf{r}_1,\mathbf{r}_2) = 0$ if $|\mathbf{r}_1 - \mathbf{r}_2| < 2a$ and $g(\mathbf{r}_1,\mathbf{r}_2) = 1$ otherwise, which captures the hard-particle exclusion.

IV. NUMERICAL METHODS

A. Dynamical density functional theory

Along with the initial condition and external potential, the DDFT (15) requires a free energy, which should be a functional of the density. As is standard in (D)DFT, we split up the free energy into three terms:

$$\mathcal{F}[\rho] = \mathcal{F}_{\mathrm{id}}[\rho] + \mathcal{F}_{\mathrm{ex}}[\rho] + \int \mathrm{d}\mathbf{r}\rho(\mathbf{r})V_1(\mathbf{r},t).$$

Here $\mathcal{F}_{\mathrm{id}}$ is the ideal gas free energy, namely

$$\mathcal{F}_{\mathrm{id}} = k_BT\int \mathrm{d}\mathbf{r}\rho(\mathbf{r})\big(\ln(\Lambda^3\rho(\mathbf{r})) - 1\big),$$

with Λ the thermal wavelength, which will turn out to be irrelevant, and $\mathcal{F}_{\mathrm{ex}}$ is the excess free energy. The remaining challenge is to determine a good approximation to $\mathcal{F}_{\mathrm{ex}}$. Here we choose to use Fundamental Measure Theory (FMT) for hard disks. We follow the description of Roth *et al.*[66], which is a generalisation of Rosenfeld's FMT[67], and present the formalism for a single species of hard disks, but note that it is easily extended to a mixture of different species/sizes. Our numerical scheme also allows the straightforward implementation of any other FMT, such as the White Bear version[68]; see Ref. 69 for a recent review of FMT.

The calculation of the FMT free energy proceeds in two steps. First we define a set of weighted densities n_α, which are convolutions of weight functions ω_α with the density:

$$n_\alpha(\mathbf{r}) = \int \mathrm{d}\mathbf{r}' \rho(\mathbf{r}')\omega_\alpha(\mathbf{r}-\mathbf{r}').$$

These weighted densities are then combined through a function Υ, which is then integrated to give the excess free energy

$$\mathcal{F}_{\mathrm{ex}} = k_B T \int \mathrm{d}\mathbf{r} \Upsilon(\{n_\alpha(\mathbf{r})\}).$$

We note that the functional derivative of $\mathcal{F}_{\mathrm{ex}}$ may be calculated through the expression

$$\frac{\delta \mathcal{F}_{\mathrm{ex}}}{\delta \rho(\mathbf{r})} = k_B T \sum_\alpha \Big(\frac{\partial \Upsilon}{\partial n_\alpha} * \hat{\omega}_\alpha \Big)(\mathbf{r}),$$

where $*$ denotes convolution and $\hat{\omega}_\alpha(\mathbf{r}) = \omega_\alpha(-\mathbf{r})$.

The choices of ω_α and Υ depend on the particular version of FMT. Here, recalling that the radius of the disk is denoted by a, we have five weights

$$\begin{aligned}
\omega_0(\mathbf{r}) &= \delta(a-|\mathbf{r}|)/(2\pi a) \\
\omega_2(\mathbf{r}) &= \delta(a-|\mathbf{r}|), \\
\boldsymbol{\omega}_2^{(1)}(\mathbf{r}) &= \mathbf{r}\delta(a-|\mathbf{r}|), \\
\boldsymbol{\omega}_2^{(2)}(\mathbf{r}) &= (\mathbf{r}\otimes\mathbf{r})\delta(a-|\mathbf{r}|), \\
\omega_3(\mathbf{r}) &= \Theta(a-|\mathbf{r}|),
\end{aligned}$$

where δ is the Dirac-delta, Θ the Heaviside step function, and $\otimes$ denotes an outer product. Finally, we have

$$\Upsilon(\{n_\alpha\}) = -n_0 \ln(1-n_3) + \frac{1}{4\pi(1-n_3)} \Big(\frac{19}{12}(n_2)^2 - \frac{5}{12}\mathbf{n}_2^{(1)} \cdot \mathbf{n}_2^{(1)} - \frac{7}{6}\mathbf{n}_2^{(2)} \cdot \mathbf{n}_2^{(2)} \Big).$$

In order to solve the 2D DDFT equations, we follow the methods described in Ref. 70. In particular, we use pseudospectral methods to accurately and efficiently solve the equations either on the full infinite plane or on the full half space, with no truncation or periodisation required. These techniques have been shown to be very successful in a range of DFT[71–76] and DDFT[24,25,31] simulations.

In an unconfined geometry, FMT computations require integrals over circles and disks, which may be accurately and efficiently performed by pseudospectral interpolation and integration. Similarly, with our choice of g as a hard-disk cut-off, the HI terms require integration

over an infinite annulus, which is similarly straightforward. In contrast, a number of difficulties arise in the confined case. Firstly, to compute the FMT and HI integrals, we require the intersection of circles, disks and annuli with the half-space. The required collocation points are described in Ref. 70. A further difficulty is that the explicit dependence of the diffusion tensor on both particle positions (rather than only on $\mathbf{r} = \mathbf{r}_1 - \mathbf{r}_2$) means that the required integrals are no longer convolutions.

Additionally, for a hard wall at $y = 0$, it is clear that the density is zero on $y < a$. However, the support of the weighted densities for FMT is actually the entire half space. Furthermore, the derivative of the weighted densities normal to the wall exhibits a discontinuity at $y = 2a$. The discontinuities in the density and this derivative would normally seriously impact on the accuracy of pseudospectral methods. We circumvent this by splitting the half space into an infinite slit (for $y \in [0, 2a]$) and a half space $y > 2a$, which are discretized separately. Here we choose the number of collocation points in the normal direction in the strip to be the next even integer greater than $N/3$, where N is the corresponding number of points in the half space. For our simulations we find it sufficient to use a grid of 40×40 Gauss-Lobatto-Chebyshev collocation points, mapped onto the infinite or half-infinite space. To map the computational domain $[-1, 1] \otimes [-1, 1]$ to the physical domain, we consider the two coordinates separately and take the tensor product of the resulting collocation points. To map to the infinite and half-infinite lines we use

$$y_{\mathrm{I}}(x) = L\frac{x}{\sqrt{1-x^2}} \qquad \text{and} \qquad y_{\mathrm{HI}}(x) = L\frac{1+x}{1-x},$$

respectively. Here, L is an adjustable parameter; we have shown in a previous study[70] the calculations to be fairly insensitive to its value as long as it is of the same order as the lengthscale on which the density varies. For the calculations presented here, we choose $L = 3$.

A typical (confined) calculation takes around 35 minutes on an Intel Xeon E7-4830 v2 2.2GHz, of which 5 and 25 minutes are to preprocess the integration matrices for FMT and HI, respectively, 5 minutes is to find the initial (equilibrium) condition and 2 minutes is to compute the dynamics. We note that the preprocessing needs to be done only once for a given computational domain and FMT/HI formalisms and that the initial condition may be reused for various choices of HI as the equilibrium state is independent of HI. The large difference in pre-processing times for FMT and HI is due to the HI not being convolutions. In unconfined

geometries or for the Rotner-Prager case the computation times for the HI preprocessing drop to around 5 minutes. However, this pre-processing stage is completely parallelisable over the collocation points, and is thus not a significant bottleneck in applications.

B. Stochastic dynamics

As discussed by Ermak and McCammon[77], one may construct fixed time step realisations of the stochastic process described by the Smoluchowski equation (1) via a stochastic differential equation for the positions of the particles:

$$\mathbf{r}_i(t+\Delta t) = \mathbf{r}_i(t) + \sum_{j=1}^{N} \boldsymbol{\nabla}_{\mathbf{r}_j} \cdot \mathbf{D}_{ji}(\mathbf{r}^N, t)\Delta t + \frac{1}{k_B T} \sum_{j=1}^{N} \mathbf{D}_{ij}(\mathbf{r}^N, t) \boldsymbol{\nabla}_{\mathbf{r}_j} V(\mathbf{r}^N, t)\Delta t + \mathbf{f}_i(\Delta t) \quad (16)$$

where the vector $\mathbf{f}(\Delta t)$ is a random displacement with a Gaussian distribution of zero mean and covariance $\langle \mathbf{f}_i(\Delta t)\mathbf{f}_i(\Delta t)\rangle = 2\mathbf{D}_{ij}\Delta t$. Since $\mathbf{D}_{ij}$ is a function of $\mathbf{r}^N$, the noise in (16) is mulitplicative, and thus we need to consider which stochastic calculus we are using. As discussed by Ermak anc McCammon[77], all quantities should be determined using the positions at the start of the time step (which is computationally attractive as the equations are then explicit). Lançon *et al.*[78] found that the convention is determined by the physics of the system. In fact, it corresponds to neither the standard Ito nor Stratonovich calculus, but to evaluating the diffusion tensor at the end of the time step, termed the 'isothermal calculus'. Equation (16) is then obtained by expanding $\mathbf{D}(x + \Delta x) \approx \mathbf{D}(x) + \boldsymbol{\nabla} \cdot \mathbf{D}\Delta x$, which explains the additional drift term, which would not be present if one used the Ito calculus. As discussed previously, the 3D RP and Oseen tensors are divergence-free and, in those cases, the second term on the right hand side of (16) is zero. However, for the 2D RP tensor, this is not the case and we need to use (8).

Note that both the Smoluchowski equation (1) and stochastic dynamics (16) assume that the (inter-particle) potential is differentiable. For the case of hard spheres this is not the case. As in previous work, we choose to approximate these hard-sphere interactions by a slightly softened potential. For hard spheres of radius a we define the smoothed interparticle potential (which depends only on the separation distance) by (see e.g. Ref. 26)

$$V_{\mathrm{HS}}(r) = k_B T \begin{cases} \left(\frac{2a}{r}\right)^{48} - \left(\frac{2a}{r}\right)^{24} + \frac{1}{4} & \text{if } r \leq 2^{1+1/24}a \\ 0 & \text{else.} \end{cases}$$

When dealing with systems confined by a hard wall, we use the same potential (which is now one-body) for the wall-particle interactions, but with a scaling that corresponds to particles being able to approach to within a of the wall:

$$V_{\mathrm{W-HS}}(h) = k_B T \begin{cases} \left(\frac{a}{h}\right)^{48} - \left(\frac{a}{h}\right)^{24} + \frac{1}{4} & \text{if } h \leq 2^{1/24} a \\ 0 & \text{else.} \end{cases}$$

In order to obtain the equilibrium density profiles we use slice sampling, as introduced by Neal[79], which is a Markov chain Monte Carlo algorithm that, in particular, does not require us to know the normalisation of the distribution (equivalently we do not need to know the partition function). For hard sphere dynamics this seems to be more efficient than performing a large number of stochastic simulations to obtain the equilibrium distribution. Typically the sampling takes 5 hours, whilst the dynamics take 800 hours on an Intel Xeon E7-4830 v2 2.2GHz (the dynamics are parallelisable over the number of runs).

V. NUMERICAL RESULTS

A. Validation against stochastic dynamics

We first validate our DDFT (15) by comparing to the underlying stochastic dynamics (16), firstly for an infinite, unbounded 2D domain and then for a 2D half space with a hard wall. In the following we set $D_0 = k_B T = 1$ and $a = 1/2$ (which corresponds to a particle diameter of 1). We consider a system of 50 hard spheres in a weakly-confining external potential

$$V_0 = 0.01(x^2 + z^2)$$

which is independent of time. Its purpose is simply to ensure that the particles are 'trapped', i.e. that the density goes to zero as the distance from the origin tends to infinity.

We introduce an additional, time-dependent external potential

$$V_1 = \exp(-\tau^2) V_1^A + \big(1 - \exp(\tau^2)\big) V_1^B,$$

where $\tau = t/0.01$ and

$$V_1^\alpha = -3 \exp\Big(- \frac{(x - x_\alpha)^2}{\sigma_x} - \frac{(z - z_\alpha)^2}{\sigma_z} \Big),$$

with x_α, z_α, σ_x and σ_z chosen for the particular examples. Such a potential models, for example, an optical trap[26]. However, the precise details are unimportant and the general behaviour described below is independent of the details of the potential.

In particular, in order to demonstrate the effects of HI, it is crucial that σ_x and σ_z are chosen large enough so that the wells produced by V_1 essentially contain all of the density (i.e. the 'background' density is very low). For example, if one were to have a moving potential well with a large 'background' density, the particles/density tend to move locally rather than globally, whereas the physical interpretation is much easier when one thinks of particles moving with the well.

We study this system both with and without HI. In the unbounded case we only consider the RP case, whereas in the bounded case we consider the cases with no HI, with the unbounded RP tensor and with the full diffusion tensor given by $\mathbf{D}^{\mathrm{RPB}}$ (see (9)). This allows us to demonstrate the large effects of the confinement-induced modifications to HI.

For the stochastic simulations we sample 1,000,000 configurations from the equilibrium density at $t = 0$, from which we draw 10,000 initial conditions and then perform independent simulations with step size 4×10^{-5} for the unconfined geometry and 2×10^{-5} for the confined geometry. Stochastic results are then given by averaging over all simulations.

We begin by validating our DDFT against the underlying stochastic dynamics in an unconfined geometry. We set $x_A = -2$, $z_A = -2$, $x_B = 0$, $z_B = 2$ and $\sigma_x = \sigma_z = 50$. Snapshots of the DDFT density for the case with no HI (top, red) and with RP HI (bottom, blue) are given in Figures 3–5. Left plots show the density as a surface, with the equivalent contour plots on the right, with arrows showing the flux (the term inside the divergence in (12)). The background shading on the contour plots denotes the error between the stochastic simulations and the DDFT. We note that this grows over time, but still remains relatively small. For example, the relative L^2 errors between the DDFT and stochastic simulations for the case with no HI are 8.4×10^{-4}, 0.0093 and 0.0361 for the snapshots at $t = 0$, 1 and 2, respectively. I.e. the relative error is at most a few percent. The equivalent values for the case with RP HI are 8.4×10^{-4}, 0.0361 and 0.0861, which, whilst not quite as accurate, are still acceptable, especially given the vast difference in computation time, as described in the previous section. We leave the interpretation of the results for the next section and now discuss the analogous validation for the confined geometry.

Figures 6–8 show the equivalent results for a confined geometry with $x_A = 0$, $z_A = 8$,

$x_B = 0$, $z_B = 4$, $\sigma_x = 250$ and $\sigma_z = 50$. Along with the case with no HI (red, top) and the unbounded RP HI (middle, blue), we also show the results for the full HI including the wall effects (bottom, magenta). For comparison, the relative L^2 errors for $t = 0$, 0.33 and 0.66 are, for the case with no HI, 0.0018, 0.0023 and 0.0048, respectively. The corresponding values for the RP case are 0.0018, 0.0105 and 0.0312, and finally, for the case with the full HI they are 0.0018, 0.0066 and 0.0195. Once again these relative errors are no more than a few percent, demonstrating very good agreement between the stochastic dynamics and the DDFT.

B. Effects of hydrodynamic interactions

Having validated our DDFT, in this subsection we will discuss the effects of the various choices of HI using the DDFT results. In addition to those already discussed and shown in Figures 3–8, we have also looked at the case where the density is moved away from the wall with parameters $x_A = 0$, $z_A = 6$, $x_B = 0$, $z_B = 8$, $\sigma_x = 250$ and $\sigma_z = 50$. The corresponding results are shown in Figures 9–11.

Our first observation is that, in the unbounded geometry (Figs 3–5). the inclusion of RP HI tends to enhance the collective motion of the particles. This fundamentally changes the dynamics of the system compared to the case with no HI, and demonstrates that it is essential to include the effects of HI in such colloidal systems. From Figs 6–11 we see that this is also the case in the bounded domain; the inclusion of HI on the RP level actually ignores all the effects of the wall, so this is to be expected. Once again, the dynamics significantly differ from those when HI are neglected. However, we also see that both these dynamics are different to those when the full RPB HI for a confined system is included. These HI have two main effects: (i) Away from the wall they behave like RP HI and hence enhance the collective motion. (ii) Near to the wall, these HI retard motion both towards and away from the wall. When moving groups of particles towards or away from the wall these two effects are in direct competition. It is clear that the RP formalism significantly overestimates the motion-enhancing effects present in a confined system, which is more accurately modelled by the RPB HI. This can be seen from Fig. 12 where we plot the density profile at the wall for each of the three choices of HI. The top row shows the wall densities when the motion is 'towards' the wall; here we see that RP HI significantly overestimate the density at the

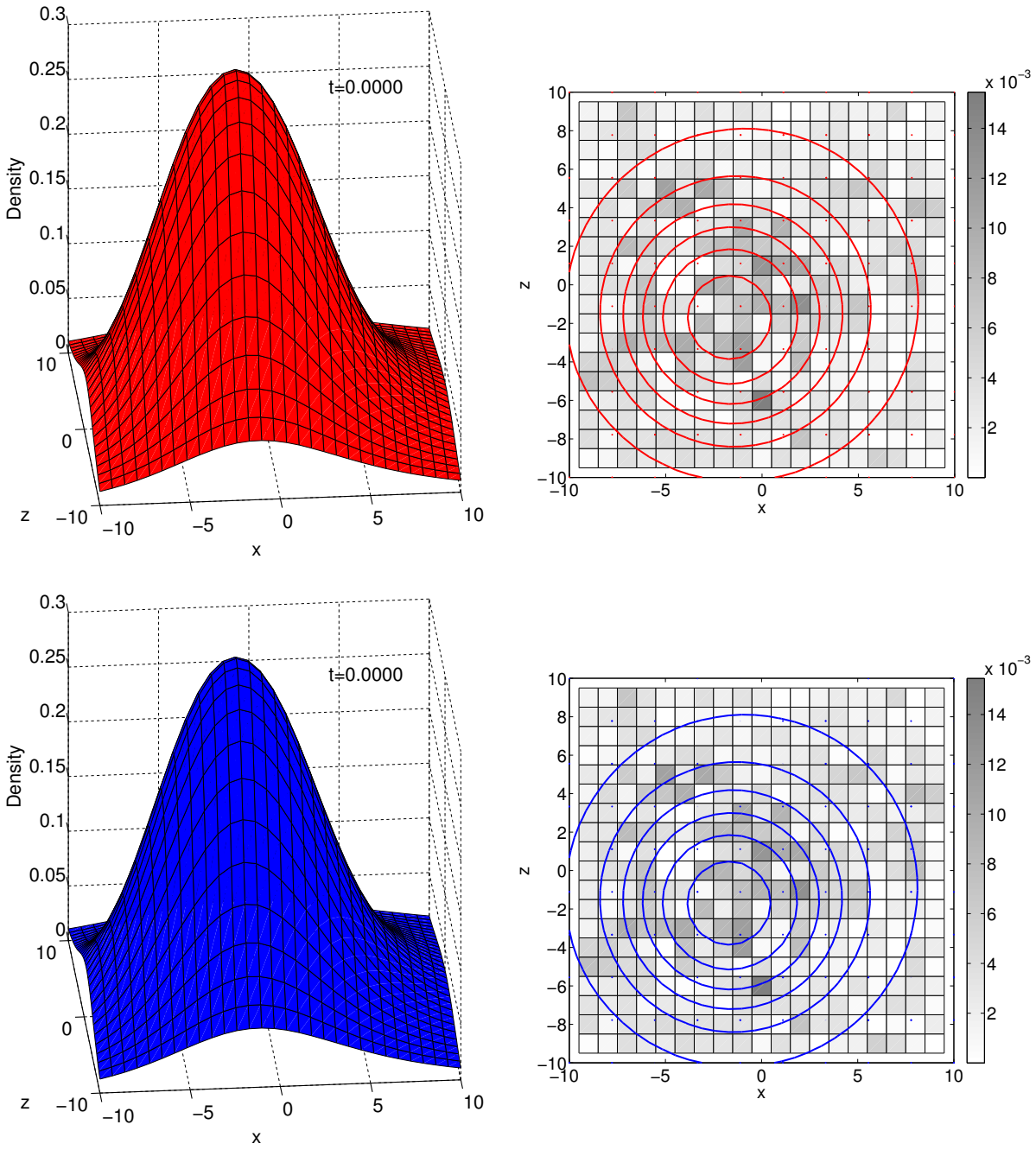

FIG. 3. Density snapshots at $t = 0$ for an unconfined geometry. Left plots show the density as a surface; top (red) for no HI and bottom (blue) for RP HI. Right plots show the corresponding contours. Arrows (which are all of zero length in this plot) indicate the density flux. Shading denotes the difference between the DDFT results and the corresponding stochastic simulations. Note that, since we choose the same initial condition for both computations, the top and bottom figures are identical, but this will not be the case in later plots.

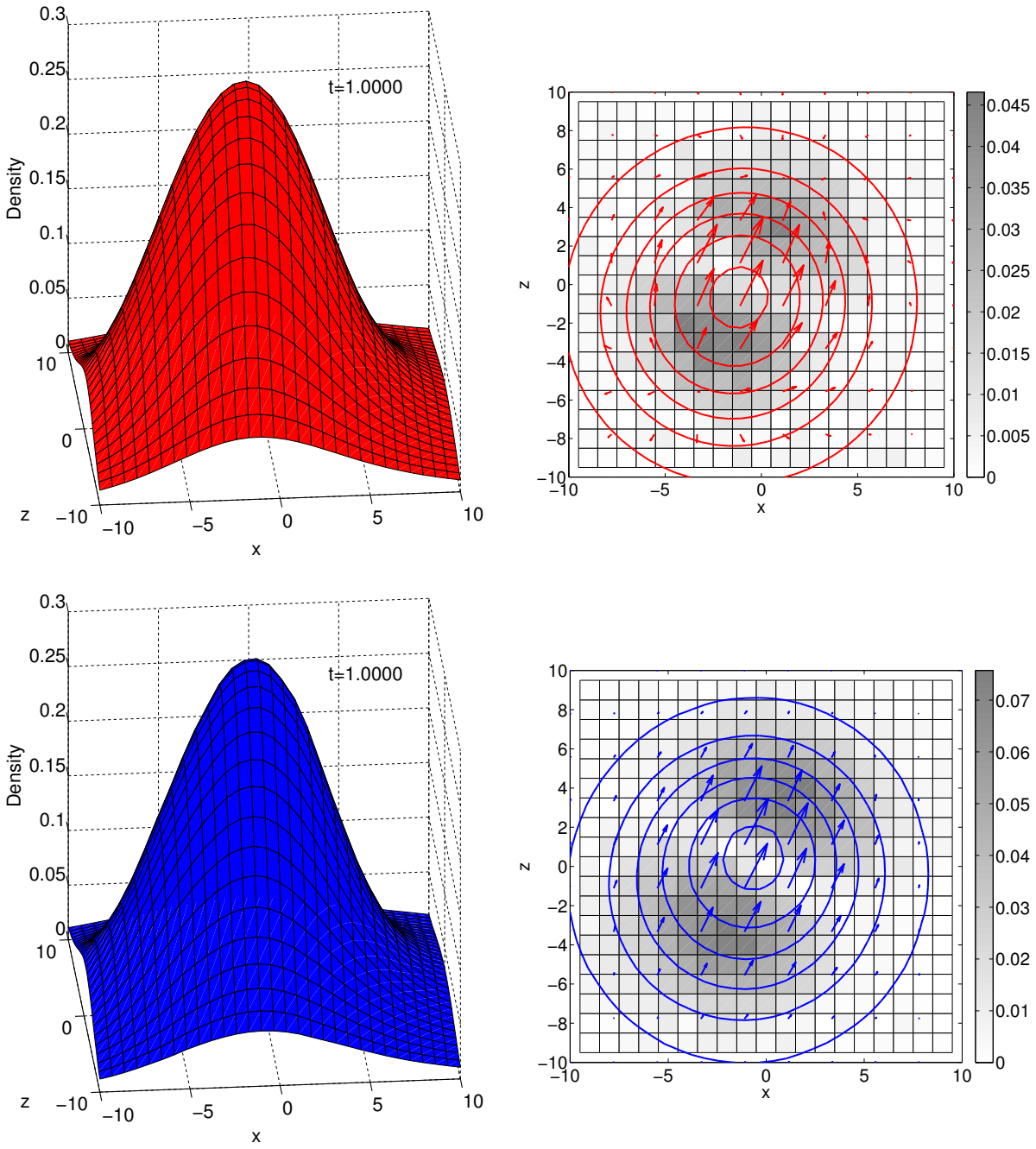

FIG. 4. As Fig. 3 for $t = 1$.

wall. As described, the correct behaviour involves a balance of the enhancing effects of RP and retarding effects of the wall HI, which, in this case lead to a slight enhancement at the wall when compared to no HI. The case for motion 'away' from the wall (bottom row) is analogous.

Finally looking at the fluxes (arrows in Figs 6–11), we see that HI modify the overall

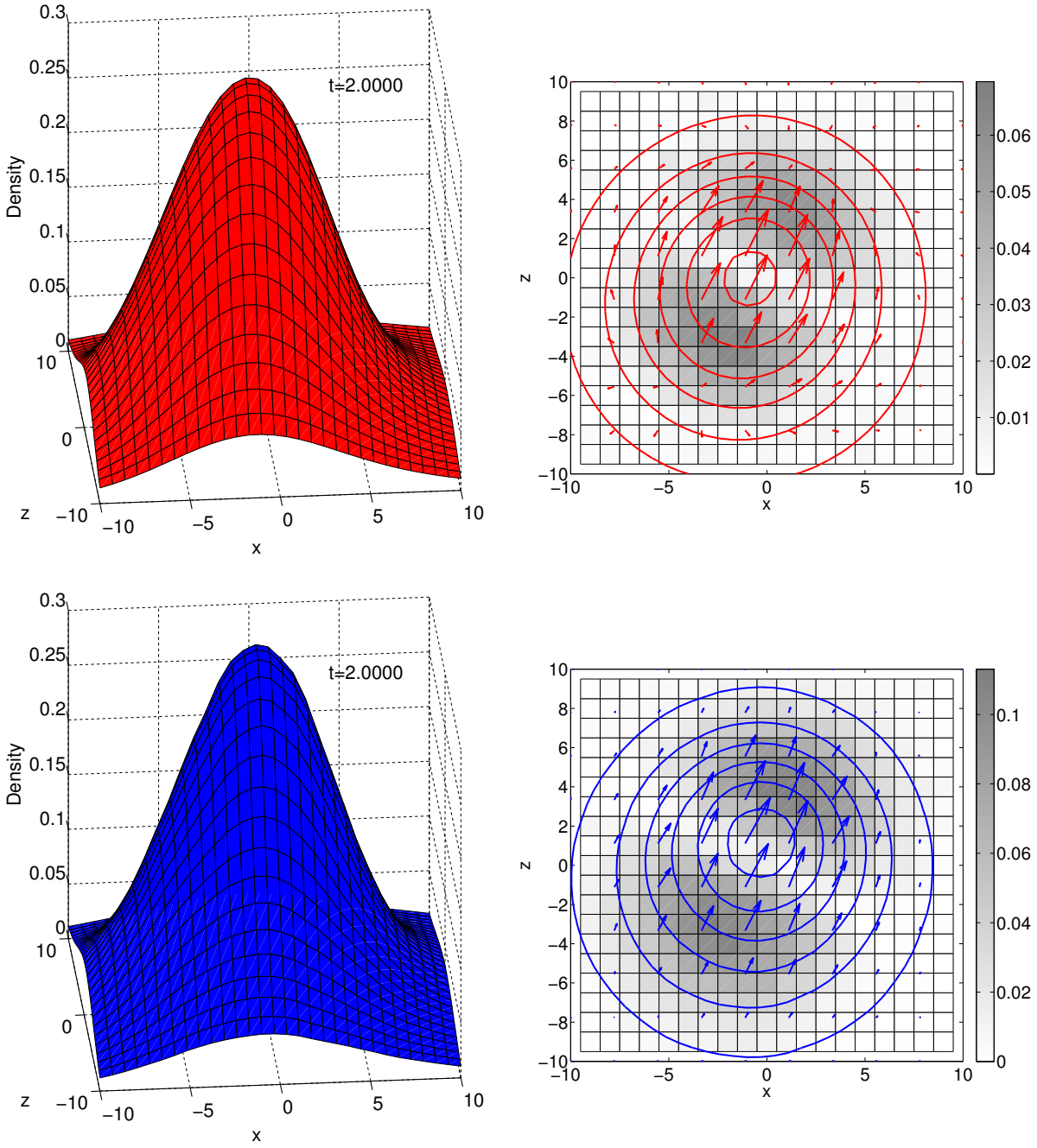

FIG. 5. As Fig. 3 for $t = 2$.

motion of the particles. For the cases without HI, the flux is predominantly directed perpendicular to the wall. When including HI, there is far more 'bending' of the streamlines, which is particularly obvious in the fluxes for large $|x|$ in Fig 11.

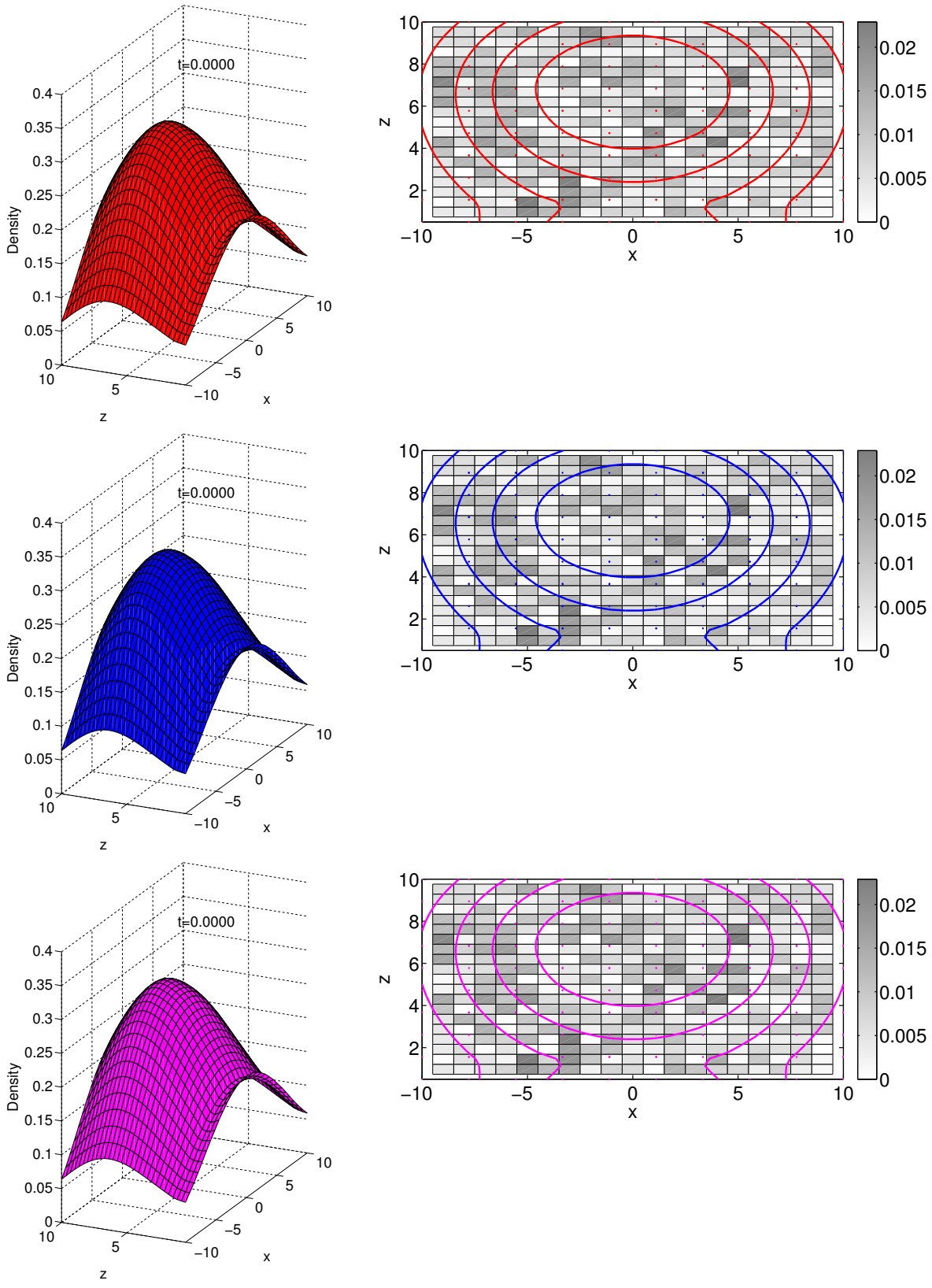

FIG. 6. As Fig. 3, but for a confined geometry with a hard wall at $z = 0$, for $t = 0$. The top (red) plots show results for no HI, the middle (blue) for RP HI and the bottom (magenta) for RPB HI.

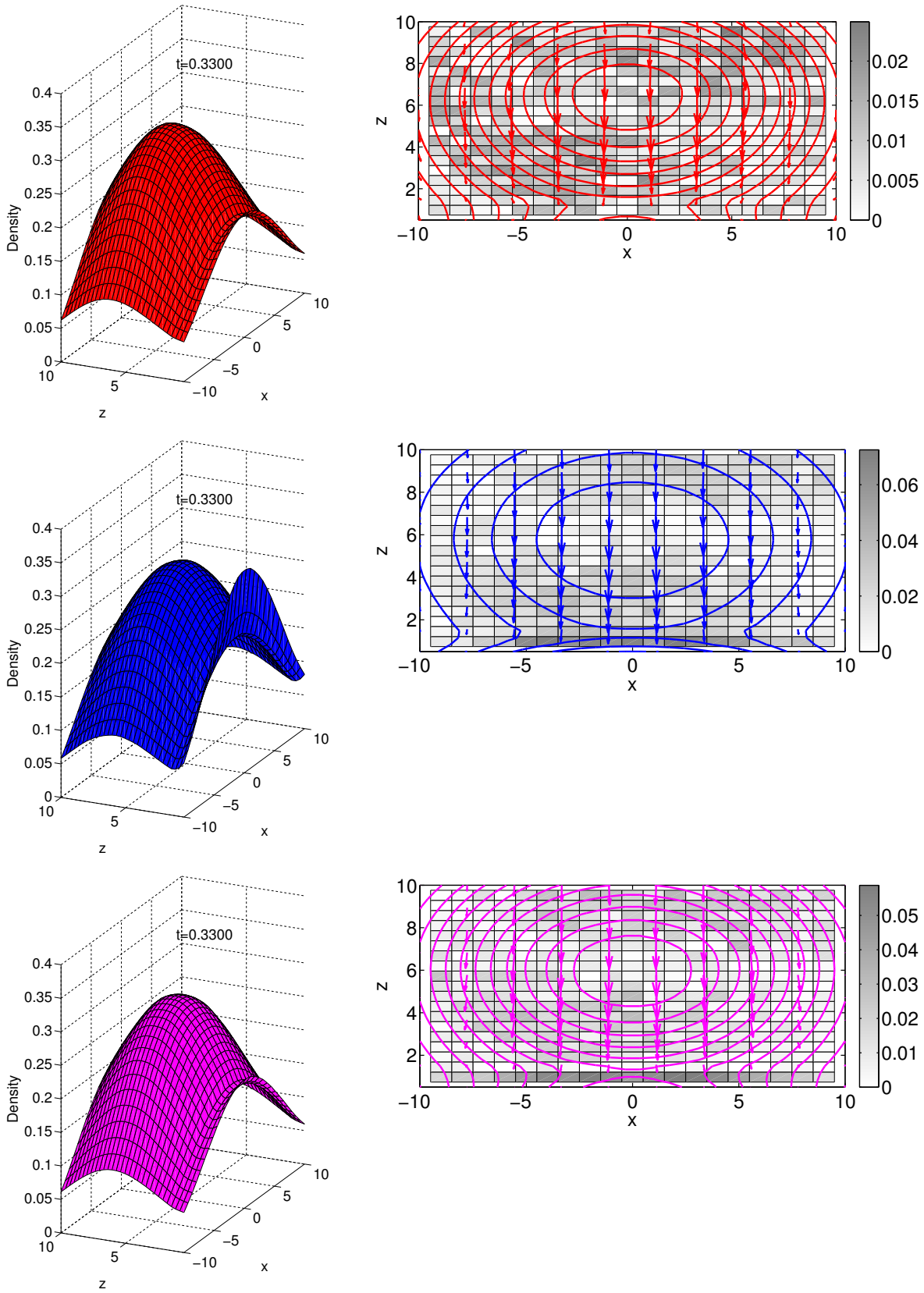

FIG. 7. As Fig. 6 for $t = 0.33$.

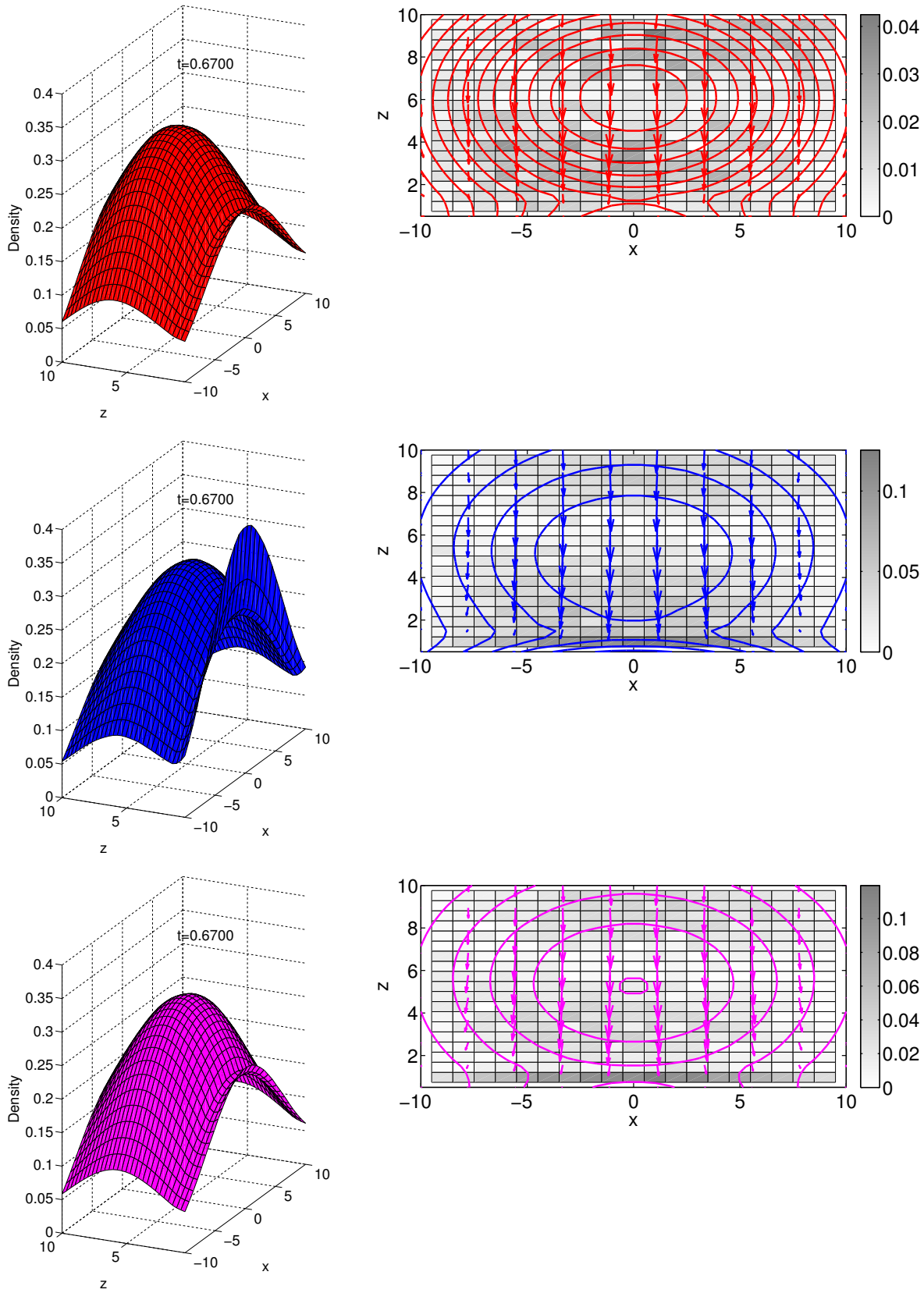

FIG. 8. As Fig. 6 for $t = 0.67$.

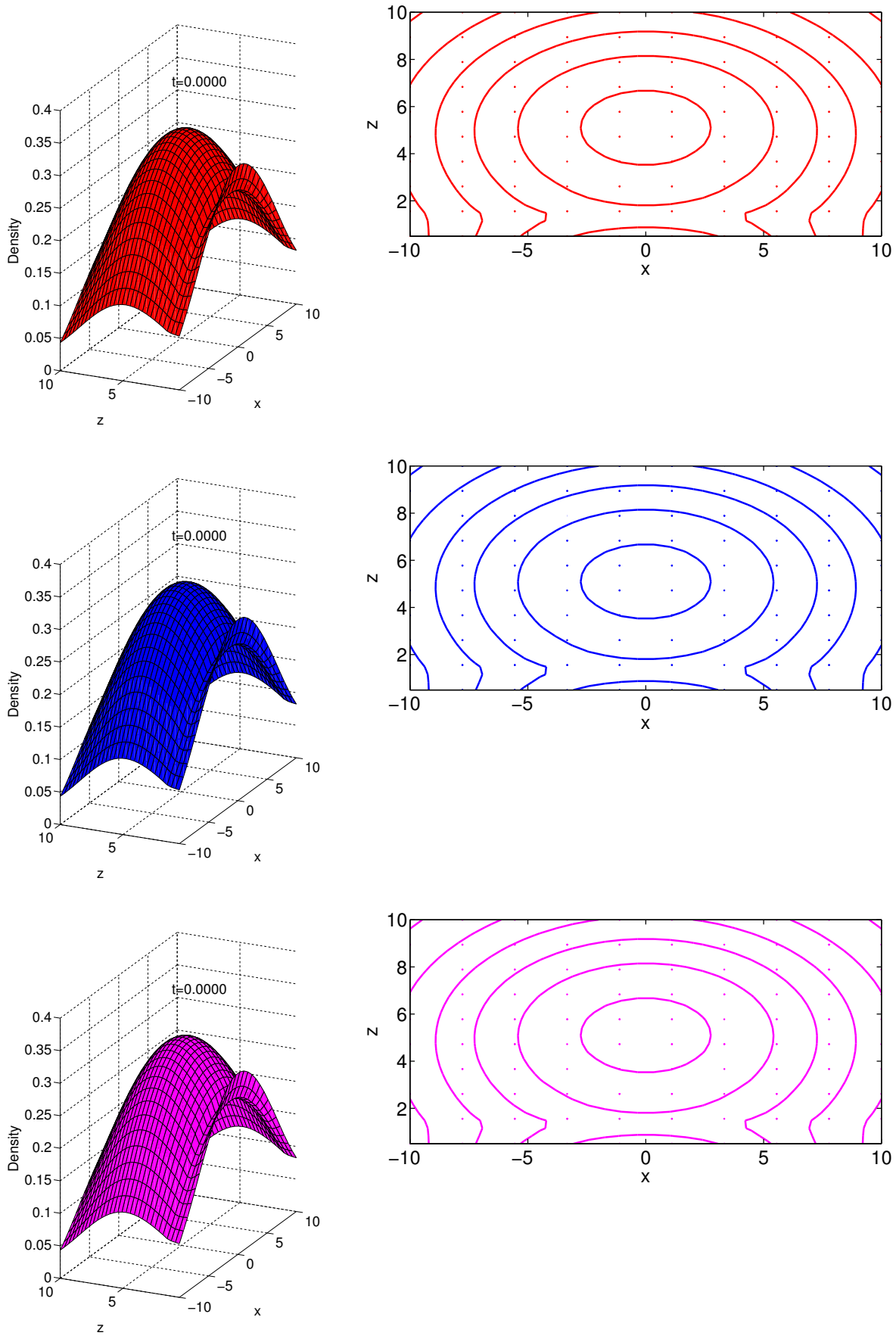

FIG. 9. As Fig. 6 for $t = 0$, but with a potential moving away from the wall. Note that, due to the computational expense of performing the stochastic simulations, we do not show those results here.

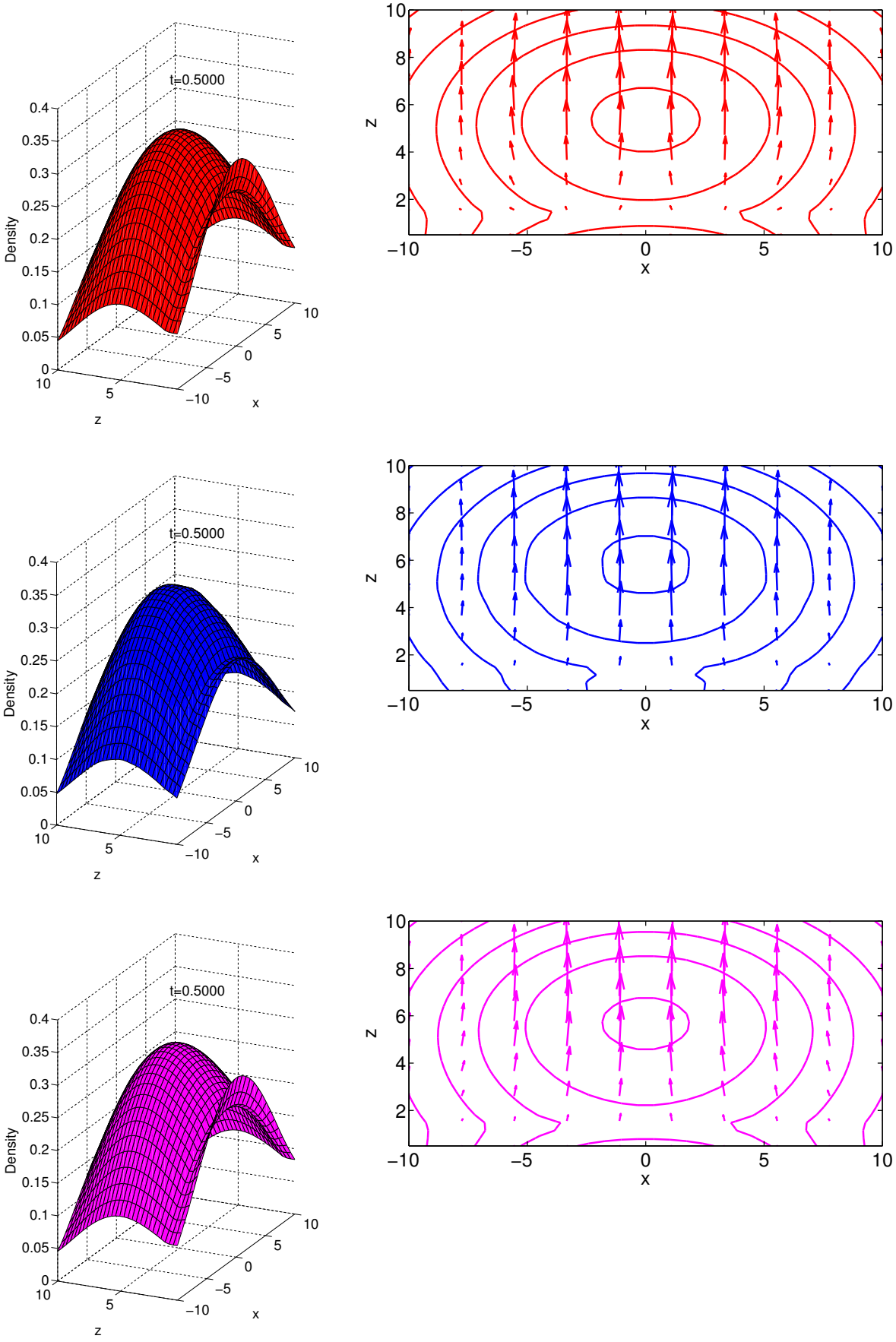

FIG. 10. As Fig. 9 for $t = 0.5$.

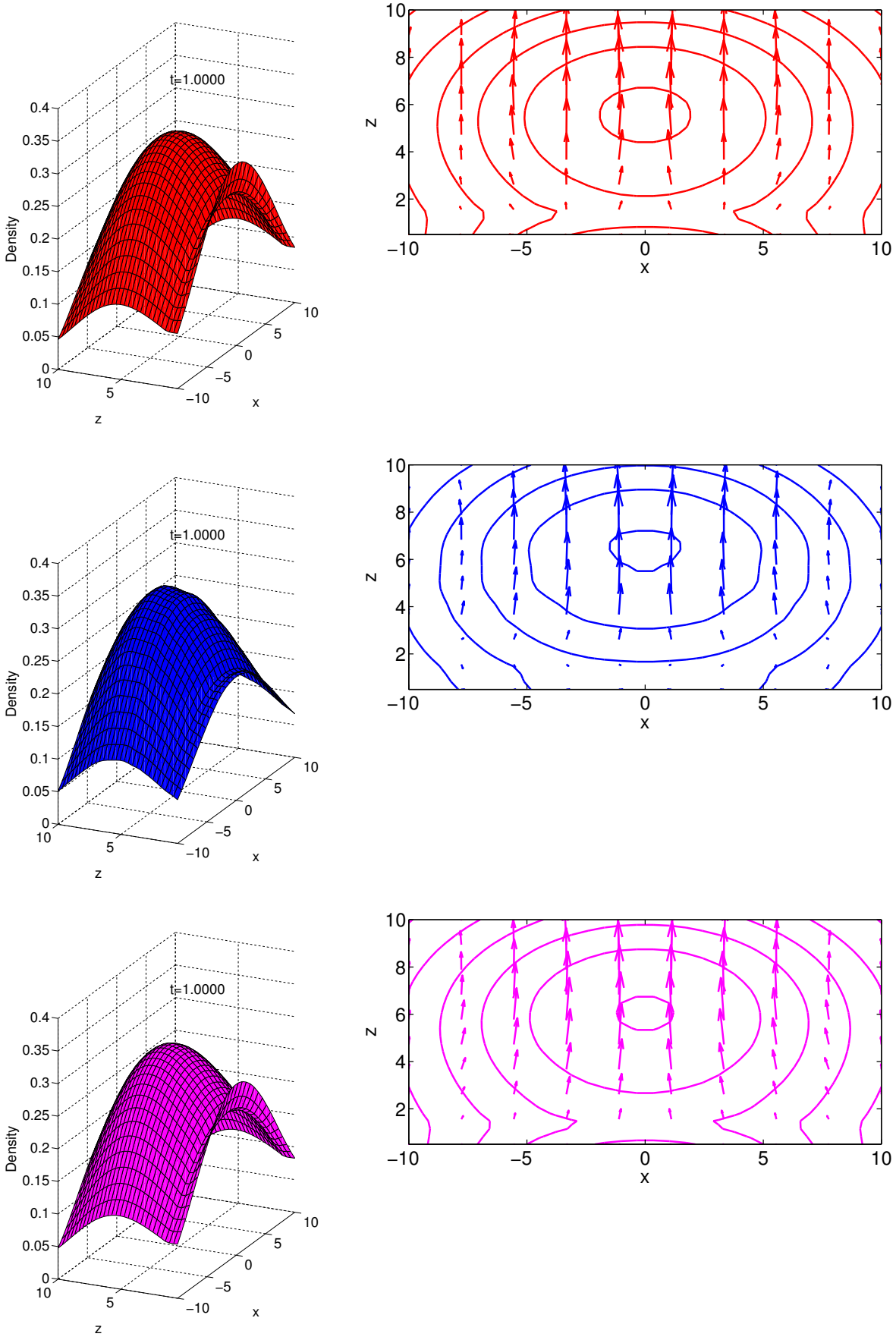

FIG. 11. As Fig. 9 for $t = 1$.

VI. CONCLUSIONS AND OUTLOOK

We have derived a DDFT for confined geometries, including HI and demonstrated its accuracy when compared to the underlying stochastic dynamics, which are computationally much less tractable for large numbers of particles. We have also demonstrated that, in order to reproduce the correct physics, it is crucial to include the wall-induced effects of HI. For example, we have shown that, close to the wall, including the effect of the wall on HI, significantly reduces the collective motion-enhancing effect of RP HI. An accurate description of these effects is therefore important when trying to quantitatively predict adsorption and desorption of colloidal particles.

Future important extensions of this work are to: (i) Extend the HI description to infinite channels and to completely confined geometries, which will significantly increase the industrial and real-world applications of DDFT; (ii) Include lubrication HI forces, which become significant at higher particle densities; (iii) Derive and implement the DDFT for anisotropic particles and for multiple species of differently-sized/shaped particles. (iv) Include the effects of an external flow. (v) Derive analogous DDFTs which include the (microscopic) inertia of the colloidal particles. (vi) Extend the numerical scheme to 3D. We believe that this work is a first step in transforming DDFT from a tool of mainly theoretical interest applied to model problems to a useful tool for applications.

ACKNOWLEDGMENTS

We acknowledge financial support from Imperial College through a DTG International Studentship, the European Research Council via Advanced Grant No. 247031 and the Engineering and Physical Sciences Research Council of the UK via Grant No. EP/L025159/1. We are grateful to Drs Nikos Savva and Peter Yatsyshin for stimulating discussions on DDFT and spectral methods.

Appendix A: Divergence of 3D hydrodynamic interaction tensors in 2D

For unbounded geometries, the term we require for the stochastic dynamics is

$$\mathbf{d}_i = \sum_j \boldsymbol{\nabla}_{\mathbf{r}_j} \cdot \mathbf{D}^{\mathrm{RP}}_{ji}(\mathbf{r}_i, \mathbf{r}_j) = -\sum_j \boldsymbol{\nabla}_{\mathbf{r}} \cdot \mathbf{D}^{\mathrm{RP}}_{ji}(\mathbf{r}), \tag{A1}$$

where we have used the chain rule to obtain the second expression. Note that this term is zero in the full 3D geometry, but partial confinement results in the divergence no longer vanishing. For completeness we treat the RP tensor in d dimensions, where we are particularly interested in the case $d = 2$. For ease of notation we suppress the superscript and write the α, β component of $\mathbf{D}_{ji}^{\mathrm{RP}}$ as

$$D_{ij}^{\alpha\beta}(\mathbf{r}) = \frac{\delta_{ij}\delta_{\alpha\beta}}{6\pi\eta a} + (1-\delta_{ij})\frac{1}{8\pi\eta}\Big[\frac{\delta_{\alpha\beta}}{r} + \frac{r_\alpha r_\beta}{r^3} + \frac{2a^2}{3}\Big(\frac{\delta_{\alpha\beta}}{r^3} - 3\frac{r_\alpha r_\beta}{r^5}\Big)\Big].$$

Using the definition of the divergence of a tensor $\mathbf{D}$, namely $(\boldsymbol{\nabla}_{\mathbf{r}}\cdot\mathbf{D})_\beta = \sum_\alpha \frac{\partial D^{\beta\alpha}}{\partial r_\alpha}$ we require

$$\frac{\partial D^{\beta\alpha}}{\partial r_\alpha} = \frac{1-\delta_{ij}}{8\pi\eta}\Big[\frac{r_\beta}{r^3} - 3\frac{r_\alpha^2 r_\beta}{r^5} + \frac{2a^2}{3}\Big(-6\frac{\delta_{\alpha\beta}r_\alpha}{r^5} - 3\frac{r_\beta}{r^5} + 15\frac{r_\alpha^2 r_\beta}{r^7}\Big)\Big]$$

and hence find

$$\begin{aligned}(\boldsymbol{\nabla}_{\mathbf{r}}\cdot\mathbf{D}_{ij})_\beta &= \frac{1-\delta_{ij}}{8\pi\eta}\sum_{\alpha=1}^{d}\Big[\frac{r_\beta}{r^3} - 3\frac{r_\alpha^2 r_\beta}{r^5} + \frac{2a^2}{3}\Big(-6\frac{\delta_{\alpha\beta}r_\alpha}{r^5} - 3\frac{r_\beta}{r^5} + 15\frac{r_\alpha^2 r_\beta}{r^7}\Big)\Big]\\ &= \frac{1-\delta_{ij}}{8\pi\eta}\Big[\frac{r_\beta}{r^3} - 2a^2\frac{r_\beta}{r^5}\Big]\end{aligned}$$

and so, reintroducing the superscript,

$$\boldsymbol{\nabla}_{\mathbf{r}}\cdot\mathbf{D}_{ij}^{\mathrm{RP}} = \frac{1-\delta_{ij}}{8\pi\eta}(d-3)\Big[\frac{1}{r^3} - 2a^2\frac{1}{r^5}\Big]\mathbf{r},$$

where the particular form of (8) is given by setting $d = 2$. It follows that $\mathbf{d}_i$ from (A1) is given by

$$\mathbf{d}_i = \sum_j \frac{1-\delta_{ij}}{8\pi\eta}(3-d)\Big[\frac{1}{r_{ij}^3} - 2a^2\frac{1}{r_{ij}^5}\Big]\mathbf{r}_{ij}.$$

For geometries confined by a single hard wall, in the full 3D system the divergence of all but the self-mobility term vanish. For the self-mobility, it is easy to see that

$$\boldsymbol{\nabla}_{\mathbf{r}}\cdot\mathbf{D}_{\mathrm{self}}^{\mathrm{RPB}} = \frac{1}{6\pi\eta a}\Big(\frac{9a}{16z^2} - \frac{3a^3}{8z^4}\Big)\hat{\mathbf{z}},$$

where $\hat{\mathbf{z}}$ is the unit vector in the z-direction.

When confined to 2D we find that, for $\alpha \in \{x, y\}$,

$$\begin{aligned}(\boldsymbol{\nabla}_{\mathbf{r}}\cdot\mathbf{D}_{ij}^{\mathrm{RPB}})_\alpha &= \frac{1}{8\pi\eta}R_\alpha\Big(6z_i z_j\frac{1}{R^5} - \frac{1}{R^3}\Big) + \frac{a^2}{4\pi\eta}R_\alpha\Big(-\frac{5R_z^2}{R^7} + \frac{1}{R^5}\Big)\\ (\boldsymbol{\nabla}_{\mathbf{r}}\cdot\mathbf{D}_{ij}^{\mathrm{RPB}})_z &= \frac{1}{8\pi\eta}\Big(\frac{2z_j}{R^3} - \frac{R_z}{R^3}\Big) + \frac{a^2}{4\pi\eta}R_z\Big(-\frac{5R_z^2}{R^7} + \frac{1}{R^5}\Big)\end{aligned}$$

Appendix B: Derivation of DDFT

We compute $N\int \mathrm{d}\mathbf{r}^{N-1}(1)$, giving

$$\frac{\partial\rho(\mathbf{r}_1,t)}{\partial t} = N\boldsymbol{\nabla}_{\mathbf{r}_1}\cdot\int \mathrm{d}\mathbf{r}^{N-1}\Big[\mathbf{D}^{(0)}(\mathbf{r}_1)+\sum_{k\neq 1}\mathbf{D}^{(1)}(\mathbf{r}_1,\mathbf{r}_k)\Big]\Big[\boldsymbol{\nabla}_{\mathbf{r}_1}+\frac{1}{k_BT}\boldsymbol{\nabla}_{\mathbf{r}_1}V(\mathbf{r}^N,t)\Big]\rho^{(N)}(\mathbf{r}^N,t)$$
$$+ N\boldsymbol{\nabla}_{\mathbf{r}_1}\cdot\int \mathrm{d}\mathbf{r}^{N-1}\sum_{j\neq 1}\mathbf{D}^{(2)}(\mathbf{r}_1,\mathbf{r}_j)\Big[\boldsymbol{\nabla}_{\mathbf{r}_j}+\frac{1}{k_BT}\boldsymbol{\nabla}_{\mathbf{r}_j}V(\mathbf{r}^N,t)\Big]\rho^{(N)}(\mathbf{r}^N,t),$$

where we have used the divergence theorem to remove any terms with $i\neq 1$. Now, by symmetry of $\rho^{(N)}$ and V under interchange of the dummy variables of integration, we may remove the sums to give factors of $N-1$, giving

$$\frac{\partial\rho(\mathbf{r}_1,t)}{\partial t} = N\boldsymbol{\nabla}_{\mathbf{r}_1}\cdot\Big(\mathbf{D}^{(0)}(\mathbf{r}_1)\int \mathrm{d}\mathbf{r}^{N-1}\Big[\boldsymbol{\nabla}_{\mathbf{r}_1}+\frac{1}{k_BT}\boldsymbol{\nabla}_{\mathbf{r}_1}V(\mathbf{r}^N,t)\Big]\rho^{(N)}(\mathbf{r}^N,t)\Big) \tag{B1}$$
$$+ N(N-1)\boldsymbol{\nabla}_{\mathbf{r}_1}\cdot\int \mathrm{d}\mathbf{r}_2\mathbf{D}^{(1)}(\mathbf{r}_1,\mathbf{r}_2)\int \mathrm{d}\mathbf{r}^{N-2}\Big[\boldsymbol{\nabla}_{\mathbf{r}_1}+\frac{1}{k_BT}\boldsymbol{\nabla}_{\mathbf{r}_1}V(\mathbf{r}^N,t)\Big]\rho^{(N)}(\mathbf{r}^N,t)$$
$$+ N(N-1)\boldsymbol{\nabla}_{\mathbf{r}_1}\cdot\int \mathrm{d}\mathbf{r}_2\mathbf{D}^{(2)}(\mathbf{r}_1,\mathbf{r}_2)\int \mathrm{d}\mathbf{r}^{N-2}\Big[\boldsymbol{\nabla}_{\mathbf{r}_2}+\frac{1}{k_BT}\boldsymbol{\nabla}_{\mathbf{r}_2}V(\mathbf{r}^N,t)\Big]\rho^{(N)}(\mathbf{r}^N,t).$$

As mentioned in the main text, the next step is to rewrite the terms involving the N-body potential as functionals of ρ via the excess free energy.

For this we consider an out-of-equilibrium system at $t=t_0$ with instantaneous density $\rho(\mathbf{r},t_0)$ and N-body density $\rho^{(N)}(\mathbf{r}^N,t_0)$. From time-independent DFT, we know that every equilibrium density $\rho_0(\mathbf{r})$ is associated with a unique external potential $\Phi(\mathbf{r})$. We may now identify the instantaneous out-of-equilibrium density with an equilibrium density in a corresponding reference system with external potential $\Phi(\mathbf{r},t_0)=V_1(\mathbf{r},t_0)+U(\mathbf{r},t_0)$ such that $\rho_0(\mathbf{r})=\rho(\mathbf{r},t_0)$. This holds for each point in time with the external potential $U(\mathbf{r},t)$ and instantaneous density $\rho_t(\mathbf{r})$ parametrized by t. It follows that the full N-body density is also at equilibrium under the addition of the N-body external potential $\sum_{n=1}^{N}U(\mathbf{r}_n)$.

In the reference equilibrium system we have

$$\frac{k_BT\boldsymbol{\nabla}_{\mathbf{r}}\rho_t(\mathbf{r})}{\rho_t(\mathbf{r})}+\boldsymbol{\nabla}_{\mathbf{r}}\Phi(\mathbf{r},t) = -\boldsymbol{\nabla}_{\mathbf{r}}\frac{\delta\mathcal{F}_{\mathrm{ex}}[\rho]}{\delta\rho}\Big|_{\rho=\rho_t},$$

where $\mathcal{F}_{\mathrm{ex}}$ is the excess free energy. From this we easily see that

$$\boldsymbol{\nabla}_{\mathbf{r}}U(\mathbf{r},t) = -\boldsymbol{\nabla}_{\mathbf{r}}\frac{\delta\mathcal{F}[\rho]}{\delta\rho(\mathbf{r},t)} \tag{B2}$$

with

$$\mathcal{F}[\rho] = k_BT\int \mathrm{d}\mathbf{r}\rho(\mathbf{r},t)\big[\ln(\Lambda^3\rho(\mathbf{r},t)-1\big]+\mathcal{F}_{\mathrm{ex}}[\rho]+\int \mathrm{d}\mathbf{r}\rho(\mathbf{r},t)V_1(\mathbf{r},t).$$

This determines the unknown fictitious external potential U in terms of the free energy of the system. It remains to replace the N-body potential terms in the evolution equation for ρ by terms involving the free energy.

To do this we note that, at equilibrium, we have

$$\rho^{(N)}(\mathbf{r}^N) = \frac{1}{Z}\exp\Big(-\frac{1}{k_BT}\big(V(\mathbf{r}^N) + \sum_{n=1}^{N} U(\mathbf{r}_n)\big)\Big),$$

where Z is the partition function. Taking the log and then the gradient with respect to $\mathbf{r}_1$ gives

$$\begin{aligned}\boldsymbol{\nabla}_{\mathbf{r}_1}\rho^{(N)}(\mathbf{r}^N) + \frac{1}{k_BT}\rho^{(N)}(\mathbf{r}^N)\boldsymbol{\nabla}_{\mathbf{r}_1}V(\mathbf{r}^N) &= -\frac{1}{k_BT}\rho^{(N)}(\mathbf{r}^N)\boldsymbol{\nabla}_{\mathbf{r}_1}U(\mathbf{r}_1)\\ &= \frac{1}{k_BT}\rho^{(N)}(\mathbf{r}^N)\boldsymbol{\nabla}_{\mathbf{r}_1}\frac{\delta\mathcal{F}[\rho]}{\delta\rho(\mathbf{r},t)},\end{aligned} \tag{B3}$$

where we have used (B2). Evaluating $N\int \mathrm{d}\mathbf{r}^{N-1}$(B3) and $N\int \mathrm{d}\mathbf{r}^{N-1}$(B3) then gives

$$\begin{aligned}N\int \mathrm{d}\mathbf{r}^{N-1}\Big[\boldsymbol{\nabla}_{\mathbf{r}_1} + \frac{1}{k_BT}\boldsymbol{\nabla}_{\mathbf{r}_1}V(\mathbf{r}^N)\Big]\rho^{(N)}(\mathbf{r}^N) &= \frac{1}{k_BT}\rho(\mathbf{r}_1)\boldsymbol{\nabla}_{\mathbf{r}_1}\frac{\delta\mathcal{F}[\rho]}{\delta\rho(\mathbf{r}_1,t)}\\ N(N-1)\int \mathrm{d}\mathbf{r}^{N-2}\Big[\boldsymbol{\nabla}_{\mathbf{r}_1} + \frac{1}{k_BT}\boldsymbol{\nabla}_{\mathbf{r}_1}V(\mathbf{r}^N)\Big]\rho^{(N)}(\mathbf{r}^N) &= \frac{1}{k_BT}\rho^{(2)}(\mathbf{r}_1,\mathbf{r}_2)\boldsymbol{\nabla}_{\mathbf{r}_1}\frac{\delta\mathcal{F}[\rho]}{\delta\rho(\mathbf{r}_1,t)}\end{aligned}$$

We note now that the left hand side of these two equations (and the additional case of $\mathbf{r}_1 \to \mathbf{r}_2$ in the second equation) are exactly the terms in (B1), under the assumption that they also hold out of equilibrium (i.e. that the many-body densities out of equilibrium are the same as those in the corresponding equilibrium system). This is the adiabatic approximation that underlies almost all DDFTs and completes the derivation.

REFERENCES

[1]A. Einstein, Ann. Phys. Lpz **17**, 549 (1905).

[2]P. Langevin, C. R. Acad. Sci. (Paris) **146**, 530 (1908).

[3]M. Von Smoluchowski, Ann. Phys **48**, 1103 (1915).

[4]R. Brown, Phil. Mag. **4**, 161 (1828).

[5]J. Perrin, Ann. Chim. Phys. **18**, 1 (1909).

[6]A. Einstein, Ann. Phys. Lpz **324**, 289 (1906).

[7]N. Hoda and S. Kumar, J. Chem. Phys **127**, 234902 (2007).

[8]A. Wysocki and H. Löwen, J. Phys.: Condens. Matt. **23**, 284117 (2011).

[9]J. Happel and H. Brenner, *Low Reynolds Number Hydrodynamics: With Special Applications to Particulate Media*, Vol. 1 (Springer Science & Business Media, 2012).

[10]E. Lauga and T. M. Squires, Phys. Fluids **17**, 103102 (2005).

[11]G. Huber, S. A. Koehler, and J. Yang, Math. Comput. Model. **53**, 1518 (2011).

[12]B. Golshaei and A. Najafi, Phys. Rev. E **91**, 022101 (2015).

[13]G. K.-L. Chan and R. Finken, Phys. Rev. Lett. **94**, 183001 (2005).

[14]M. Schmidt and J. M. Brader, J. Chem. Phys. **138**, 214101 (2013).

[15]R. Evans, Adv. Phys. **28**, 143 (1979).

[16]E. Roman and W. Dieterich, Phys. Rev. A **32**, 3726 (1985).

[17]J.-Z. Wu, AIChE J. **52**, 1169 (2006).

[18]J.-Z. Wu and Z.-D. Li, Annu. Rev. Phys. Chem. **58**, 85 (2007).

[19]J. F. Lutsko, Adv. Chem. Phys. **144**, 1 (2010).

[20]U. M. B. Marconi and P. Tarazona, J. Chem. Phys. **110**, 8032 (1999).

[21]A. J. Archer and R. Evans, J. Chem. Phys. **121**, 4246 (2004).

[22]U. M. B. Marconi and S. Melchionna, J. Chem. Phys. **126**, 184109 (2007).

[23]A. J. Archer, J. Chem. Phys. **130**, 014509 (2009).

[24]B. D. Goddard, A. Nold, N. Savva, G. A. Pavliotis, and S. Kalliadasis, Phys. Rev. Lett **109**, 120603 (2012).

[25]B. D. Goddard, A. Nold, N. Savva, P. Yatsyshin, and S. Kalliadasis, J. Phys.: Condens. Matter **25**, 035101 (2013).

[26]M. Rex and H. Löwen, Eur. Phys. J. E **28**, 139 (2009).

[27]M. Rauscher, J. Phys.: Condens. Matt. **22**, 364109 (2010).

[28]A. J. Archer, J. Phys.: Condens. Matter **17**, 1405 (2005).

[29]R. Roth, M. Rauscher, and A. J. Archer, Phys. Rev. E **80**, 021409 (2009).

[30]K. Lichtner, A. J. Archer, and S. H. L. Klapp, J. Chem. Phys **136**, 024502 (2012).

[31]B. D. Goddard, A. Nold, and S. Kalliadasis, J. Chem. Phys. **138**, 144904 (2013).

[32]H. Wensink and H. Löwen, Phys. Rev. E **78**, 031409 (2008).

[33]A. M. Menzel, T. Ohta, and H. Löwen, Phys. Rev. E **89**, 022301 (2014).

[34]A. M. Menzel, A. Saha, C. Hoell, and H. Löwen, J. Chem. Phys. **144**, 024115 (2016).

[35]M. Rex, H. Wensink, and H. Löwen, Phys. Rev. E **72**, 021403 (2007).

[36]R. Wittkowski and H. Löwen, Mol. Phys. **109**, 2935 (2011).

[37]M. Durán-Olivencia, B. Goddard, and S. Kalliadasis, J. Stat. Phys. **164**, 785 (2016).

[38]A. A. Aerov and M. Krüger, J. Chem. Phys. **140**, 094701 (2014).

[39]U. Zimmermann, F. Smallenburg, and H. Löwen, J. Phys.: Condens. Matt. **28**, 244019 (2016).

[40]M. Rauscher, A. Domínguez, M. Krüger, and F. Penna, J. Chem. Phys. **127**, 244906 (2007).

[41]J. M. Brader and M. Krüger, Mol. Phys. **109**, 1029 (2011).

[42]J. Reinhardt, F. Weysser, and J. M. Brader, Europhys. Lett. **102**, 28011 (2013).

[43]F. Penna, J. Dzubiella, and P. Tarazona, Physical Review E **68**, 061407 (2003).

[44]U. M. B. Marconi, P. Tarazona, and F. Cecconi, J. Chem. Phys. **126**, 164904 (2007).

[45]S. van Teeffelen, C. N. Likos, and H. Löwen, Phys. Rev. Lett. **100**, 108302 (2008).

[46]J. F. Lutsko and G. Nicolis, Soft Matter **12**, 93 (2016).

[47]A. J. Archer, M. J. Robbins, and U. Thiele, Phys. Rev. E **81**, 021602 (2010).

[48]R. Wittkowski, H. Löwen, and H. R. Brand, Phys. Rev. E **82**, 031708 (2010).

[49]L. Almenar and M. Rauscher, Journal of Physics: Condensed Matter **23**, 184115 (2011).

[50]R. Wittkowski, H. Löwen, and H. R. Brand, J. Chem. Phys. **137**, 224904 (2012).

[51]D. Stopper, K. Marolt, R. Roth, and H. Hansen-Goos, Phys. Rev. E **92**, 022151 (2015).

[52]J. F. Lutsko, J. Chem. Phys. **136**, 034509 (2012).

[53]S. Kim and S. J. Karrila, *Microhydrodynamics: principles and selected applications* (Courier Corporation, 2013).

[54]J. Rotne and S. Prager, J. Chem. Phys. **50**, 4831 (1969).

[55]E. Wajnryb, K. A. Mizerski, P. J. Zuk, and P. Szymczak, Journal of Fluid Mechanics **731**, R3 (2013).

[56]H. Faxén, Ann. Phys. **373**, 89 (1922).

[57]Y. W. Kim and R. R. Netz, J. Chem. Phys. **124**, 114709 (2006).

[58]Y. von Hansen, M. Hinczewski, and R. R. Netz, J. Chem. Phys. **134**, 235102 (2011).

[59]J. Blake, in *Proc. Cambridge Philos. Soc.*, Vol. 70 (Cambridge Univ Press, 1971) pp. 303–310.

[60]M. Stimson and G. Jeffery, Proc. R. Soc. London, Ser. A **111**, 110 (1926).

[61]G. Perkins and R. Jones, Physica A **189**, 447 (1992).

[62]A. Domínguez, M. Oettel, and S. Dietrich, Phys. Rev. E **82**, 011402 (2010).

[63]J. Bleibel, A. Domínguez, and M. Oettel, J.Phys.: Condens. Matt. **28**, 244021 (2016).

[64]A. V. Straube, A. A. Louis, J. Baumgartl, C. Bechinger, and R. P. Dullens, Europhys.

Lett. **94**, 48008 (2011).

[65]M. P. Juniper, A. V. Straube, R. Besseling, D. G. Aarts, and R. P. Dullens, Nat. Commun. **6**, 7187 (2015).

[66]R. Roth, K. Mecke, and M. Oettel, J. Chem. Phys. **136**, 081101 (2012).

[67]Y. Rosenfeld, Phys. Rev. Lett. **63**, 980 (1989).

[68]R. Roth, R. Evans, A. Lang, and G. Kahl, J. Phys. Condens. Matter **14**, 12063 (2002).

[69]R. Roth, Journal of Physics: Condensed Matter **22**, 063102 (2010).

[70]A. Nold, B. D. Goddard, P. Yatsyshin, N. Savva, and S. Kalliadasis, submitted (2016).

[71]P. Yatshyshin, N. Savva, and S. Kalliadasis, Phys. Rev. E **87**, 020402(R) (2013).

[72]A. Nold, D. Sibley, B. Goddard, and S. Kalliadasis, Phys. Fluids **26**, 072001 (2014).

[73]A. Nold, D. Sibley, B. Goddard, and S. Kalliadasis, Math. Model. Nat. Phenom. **10**, 111 (2015).

[74]P. Yatshyshin, N. Savva, and S. Kalliadasis, J. Chem. Phys. **142**, 034708 (2015).

[75]P. Yatshyshin, N. Savva, and S. Kalliadasis, J. Phys.: Condens. Matter **27**, 275104 (2015).

[76]P. Yatsyshin, A. Parry, and S. Kalliadasis, J. Phys.: Condens. Matter **28**, 275001 (2016).

[77]D. L. Ermak and J. A. McCammon, J. Chem. Phys. **69**, 1351 (1978).

[78]P. Lançon, G. Batrouni, L. Lobry, and N. Ostrowsky, Europhys. Lett. **54**, 28 (2001).

[79]R. M. Neal, Ann. Stat. **31**, 705 (2003).

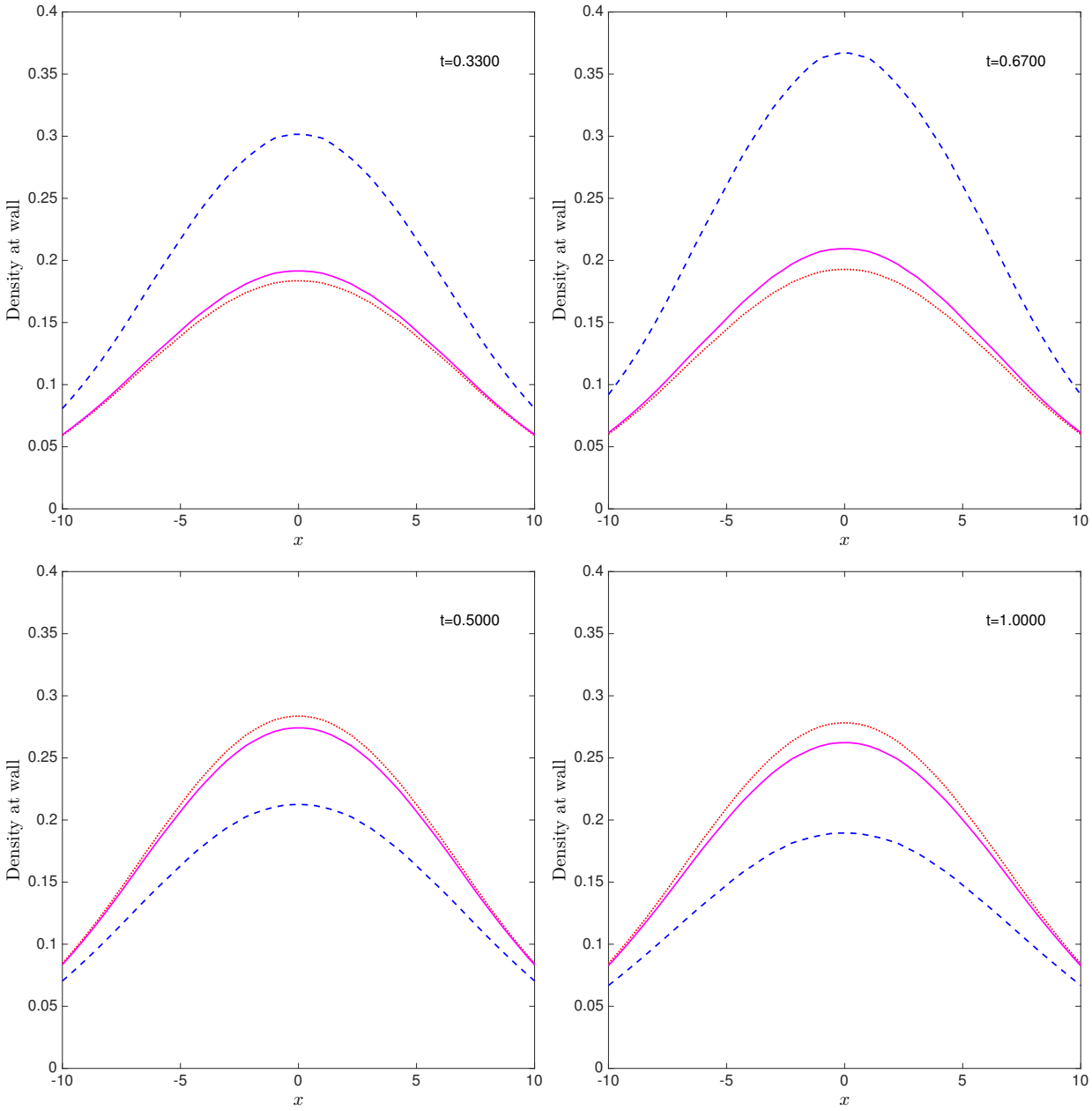

FIG. 12. Densities at the wall for no HI (red, dotted), RP HI (blue, dashed) and RPB HI (magenta, solid), for various times. Top plots are for motion 'towards' the wall (see Figs. 6–8), bottom for motion 'away' from the wall (see Figs. 9–11). Note that, within each system, each simulation starts with the same density.